The University of Edinburgh

School of Engineering

BRE Centre for Fire Safety Engineering

Academic Year 2018-19

NOVEL TESTING FOR STIFFNESS REDUCTIONS OF CROSS-LAMINATED TIMBER AT ELEVATED TEMPERATURE

Balša Jovanović

Promoter: Dr Luke Bisby

Master thesis submitted in the Erasmus+ Study Programme

International Master of Science in Fire Safety Engineering

Disclaimer

This thesis is submitted in partial fulfilment of the requirements for the degree of The International Master of Science in Fire Safety Engineering (IMFSE). This thesis has never been submitted for any degree or examination to any other University/programme. The author declares that this thesis is original work except where stated. This declaration constitutes an assertion that full and accurate references and citations have been included for all material, directly included and indirectly contributing to the thesis. The author gives permission to make this master thesis available for consultation and to copy parts of this master thesis for personal use. In the case of any other use, the limitations of the copyright have to be respected, in particular with regard to the obligation to state expressly the source when quoting results from this master thesis. The thesis supervisor must be informed when data or results are used.

Word count: 14409

Read and approved,

Balša Jovanović

30 April 2019

ABSTRACT

A novel dynamic testing method has been used to study changes in flexural elastic modulus of Cross-Laminated Timber (CLT) with elevated temperature. The elastic modulus is an important parameter for estimation of the structural response of CLT structures to fire and, using this dynamic method, it can be measured with a small, unobtrusive sensor.

A sectional analysis model was developed to estimate the reduction in stiffness of CLT beams in bending at elevated temperatures, and experiments were conducted using modal analysis in an attempt to validate the predictions made. The model comprised two parts: a two-dimensional heat transfer model that estimates the temperature profile within the CLT elements, and a stiffness reduction model which is based on the decrease in the elastic modulus of CLT at elevated temperatures along with a sectional analysis.

The model was validated by conducting experiments on four different CLT beams of dimensions 3 x 0.1 x 0.3 m. The beams were heated from ambient conditions within a specialised heating chamber capable of maintaining a gas temperature of 140 °C. Thermocouples were used to record the thermal gradients within the beam with time, and to compare these values against those predicted by the model. The reduction in dynamic flexural stiffness was measured periodically by exciting the beam and recording the response of an attached high-temperature accelerometer.

It was found that the thermal properties suggested in Eurocode 5 resulted in reasonable estimates of the temperature profiles recorded during the tests. Results also showed that most used modulus reduction models over-predicted the measured reduction of dynamic elastic modulus at elevated temperatures. The results suggest that the reduction of modulus of elasticity in timber is not only a complex function of temperature, but is also influenced by other parameters dependent on temperature such as moisture transport, cracking, and creep.

АПСТРАКТ

Нова метода динамичког тестирања је коришћена за изучавање промена у модулу еластичности при савијању греда од унакрсно ламелираног дрвета (УЛД) са повишеном температуром. Модул еластичности је важан параметар за процену структуралног понашања УЛД конструкција у пожару. Коришћењем ове динамичке методе, може се мерити малим, ненаметљивим сензором.

Модел је развијен да би се проценило смањење крутости УЛД греда при савијању при повишеним температурама, а експерименти су спроведени коришћењем модалне анализе у покушају да се потврде предвиђања. Модел се састојао из два дела: дводимензионалног модела трансфера топлоте који предвиђа температурни профил унутар УЛД елемената и модела смањења крутости који се заснива на смањењу модула еластичности УЛД при повишеним температурама заједно са анализом пресека.

Модел је валидиран спровођењем експеримената на четири различите УЛД греде димензија 3 x 0.1 x 0.3 м. Греде су грејане од амбијенталних услова унутар специјализоване грејне коморе која је могла да одржава температуру гаса од 140° C. Термопарови су коришћени за бележење топлотних градијента унутар греде током временом и за упоређивање ових вредности са онима које је предвидео модел. Смањење динамичке крутости при савијању периодично је мерено узбудљивањем греде и снимањем одговора прикаченог акцелерометра отпорног на високе температуре.

Утврђено је да су термичка својства предложена у Еурокоду 5 резултирала разумним проценама температурних профила забележених током тестирања. Резултати су такође показали да најчешће коришћени модели редукције прецењују мерено смањење динамичког модула еластичности при повишеним температурама. Резултати указују на то да смањење модула еластичности у дрвету није само комплексна функција температуре, већ је под утицајем других параметара који зависе од температуре као што су влага, напрснуће и пузање.

AGNOLEDGMENTS

I would like to thank my supervisor Dr Luke Bisby for his guidance throughout the thesis, helping me with choosing the topic and providing advice throughout my work from planning the tests to discussing results.

I would also like to thank Dr Thomas Reynolds for helping me with the modal analysis part. From explain the basics, to spending significant amount of time try to make the accelerometer work and finely helping me analyse the results.

A big thank you also goes to Felix Wiesner for showing me how to operate the heating chamber and helping me solve numerous problems during testing and advising me during the whole process.

It is also important to thank Mark Partington for all the help of setting the testing apparatus in the structures lab.

It is most essential to thank my friends James Michael Crum and Dheeraj Dilip Karyaparambil for their advice in the middle of the night, heavy lifting in the lab and listening to me talk about weird behaviour of my test samples for two weeks.

I also have to thank Farah Binte Mohd Faudzi and Arjan Dexters for helping me carry the huge timber beams multiple times without any complaints.

Contents

A	Area	h	Height of the cross section
a	Distance from centroid	I	Moment of inertia
b	Width of the cross section	k_n	Thermal conductivity in direction n
c_p	Specific heat	L	Length of the beam
E_0	Modulus of elasticity parallel to the grain	m	Mass
E_{90}	Modulus of elasticity perpendicular to the grain	m'	Mass per unit of length
		ω_n	Natural frequency
f	Frequency	ω_D	Damped natural frequency
G_r	Rolling shear modulus	ζ	Damping ratio

1. Introduction

1.1 Timber as a construction material

Recent trends in population growth and urbanisation are indicating growing need for housing and expanding of building infrastructure. According to "WHO | Urban population growth" (2015) urban population in 2014 accounted for 54% of the total global population, up from 34% in 1960, and continues to grow with estimation of approximately 79% by 2030. To accommodate this need it is estimated that two billion square metres of new building stock are needed every year between 2019 and 2025, especially for housing.

Traditionally steel and concrete are used as main materials for constructing tall buildings, but as global CO_2 emotions have increased by 50% in last 30 years and by some reports almost 47% of the total CO_2 emissions are inflicted by the construction process (BIS (2010)) timber should be considered as the new main construction material. The steel and concrete designs embody 26% and 57% more energy relative to the timber design, emit 34% and 81% more greenhouse gases, release 24% and 47% more pollutants into the air, discharge 400% and 350% more water pollution, produce 8% and 23% more solid waste, and use 11% and 81% more resources (from a weighted resource use perspective) (Green & Karsh (2012)). These facts coupled with recent rise of the number of tall buildings that use timber as the main structural material show that in the future timber might become a predominate construction material for tall buildings.

Fire safety concerns are a common factor that appears to distinguish between low rise and high-rise buildings. Historic fire catastrophes such as the Windsor Tower or the World Trade Centre, contributed to the development of specific safety provisions in codes and standards for high-rise buildings, such as the Society of Fire Protection Engineers (SFPE) Guideline for Very Tall Buildings SFPE (2012).

- The height is potentially beyond what fire department ladders can reach
- Building evacuation might be prolonged due to the evacuation height
- The stack effect might become a pronounced smoke spread phenomena
- Water supply limitations for fire fighting
- Challenges because of mixed occupancy of the building

- Iconic nature

It can be seen that fire safety aspect drives the limitations on the height of the tall buildings, but also that it does not discriminate any material. The biggest obstacle for tall timber buildings development is the fact that most of the building codes and fire safety regulations around the world do not allow tall buildings to be made out of combustible materials, which inevitably force all timber members to be covered by non-combustible materials, mainly plasterboards. These restrictions affect mentioned environmental and esthetical benefits that timber brings to the table. By using performance-based fire safety design framework some of these restrictions can be mended, but this requires more detailed insight into timber behaviour in elevated temperature conditions.

Compared to the steel and concrete, timber as a structural material has unique behaviour and characteristics. Firstly, in contrast to mostly isotropic steel and concrete, timber is an orthotropic material, which means that material properties differ along three mutually orthogonal axes of rotational symmetry. That as a consequence has the fact that mechanical properties in the direction of the grains are approximately ten times bigger than in the perpendicular direction.

Secondly as presented in Table 1 structurally significant material properties are lower for timber compared to its traditionally more used counterparts. Timber mechanical properties parallel to the grain are comparable with concrete, showing better behaviour in tension and worse in compression (a characteristic flaw of concrete as material) and much worse than steel. What makes timber a viable construction material for tall buildings is the fact that it is much lighter than its counterparts. With increasing height of the construction, the deadweight load increases linearly and self-weight of material plays more important role. In Table 2 mechanical properties are normalized by dividing them with the density of the material and it can be observed that timer in this way has characteristic comparable with steel and much better than concrete.

Table 1 Characteristic mechanical properties of common wood (C24), concrete (C55) and steel (S355) grades

Material	**Steel (S355)**	**Concrete (C55)**	**Softwood (C24)**
Density [kg/m³]	7850	2400	420
Strength properties [N/mm²]			
Bending	355 (Yield) 470 (Tensile)	27.0	24.0
Tension - parallel		4.2	14.5
Tension - perpendicular			0.5
Compression - parallel		55.0	21.0
Compression - perpendicular			2.5
Stiffness properties [kN/mm²]			
Modulus of elasticity	200	29	11

Timber as structural material besides being an orthotropic material is a non-homogeneous material and can contain defects such as knots or zones with different grain orientation. These irregularities can cause severe local weakening effect on mechanical properties of timber. In addition, this makes determining the mechanical properties very difficult as they can vary significantly between pieces or even within the same piece. This problem is encountered in most of the commonly used constructive materials, but is particularly pronounced in timber compared to concrete and steel.

Table 2 Wood, concrete and steel properties normalized over their density

Material	**Steel (S355)**	**Concrete (C55)**	**Softwood (C24)**
Normalized Modulus of elasticity [GPa·m³/kg]	0.025	0.012	0.026
Normalized Compression strength [kPa·m³/kg]	0.045	0.023	0.050

To remove the negative effects these irregularities can cause, Engineered Wood Products (EWP) were developed. EWP present wood products that are manufactured by binding or fixing the boards of wood, together with adhesives, or other methods of fixation to form composite materials. This way the material with better properties is made as the mentioned faults can be removed and provide more uniformity in material properties (Figure 1). In addition, the fibres of the wood can be orientated to achieve highest desired mechanical strength. The most important advantage of the EWP structural members it that they can be made in desired sizes and shapes, which may not be possible with solid wood. Moisture migration and creep are reduced due to the glue used and the various forms of layering. Each

engineering product relies on composite action between two adjacent timber plies and the glue layer adhering them together.

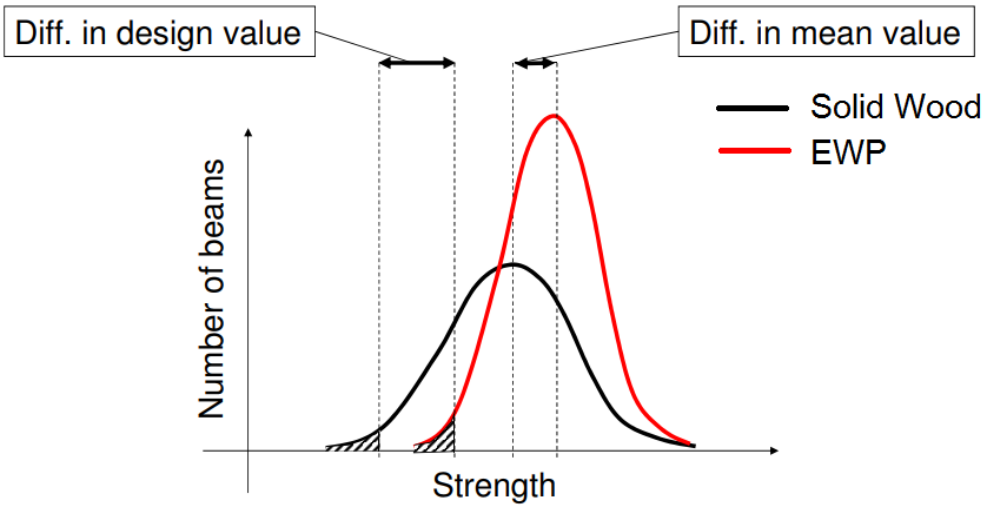

Figure 1 Better reliability representation of EWP compared to the solid wood

Several different products are available but three main products have come to dominate the market: cross-laminated timber (CLT), laminated veneer lumber (LVL) and glue laminated beams (Glulam). LVL is made of several thinly cut veneers of timber (2.5-4.4mm) glued together with the grain structure of each timber veneer oriented parallel to each other. Glulam beams are made in the same manner but with thicker plies which are approximately 30-40 mm thick. The grain direction of each of the plies is parallel and because of this, they are limited to be used only as one-way spanning members.

1.2 Cross Laminated Timber (CLT)

CLT panels consist of several layers of lumber boards stacked crosswise (typically at 90°) and glued together on their wide faces and, sometimes, on the narrow faces as well. A cross-section of a CLT element has at least three glued layers of boards placed in orthogonally alternating orientation to the neighbouring layers. In special configurations, consecutive layers may be placed in the same direction, giving a double layer (e.g., double longitudinal layers at the outer faces and/ or additional double layers at the core of the panel) to obtain specific structural capacities. CLT products are usually fabricated with an odd number of layers; three to seven layers is common and even more in some cases (Gagnon & Pirvu (2011)).

Timber is normally oriented up and down in the outer layers of CLT panels used as walls, parallel to gravity loads, to maximize the vertical load capacity of the wall. Likewise, the outer layers run parallel to the main span direction for floor and roof systems.

CLT panels used for prefabricated wall and floor structures offer many advantages. The process of cross laminating provides improved dimensional stability which easier prefabrication of elements with large dimensions. Additionally, cross laminating provides better characteristics in both directions both high in-plane and out-of-plane loading, much similar to the two-way action capability of reinforced concrete slabs. This effect also increases the splitting resistance of CLT for certain types of connection systems.

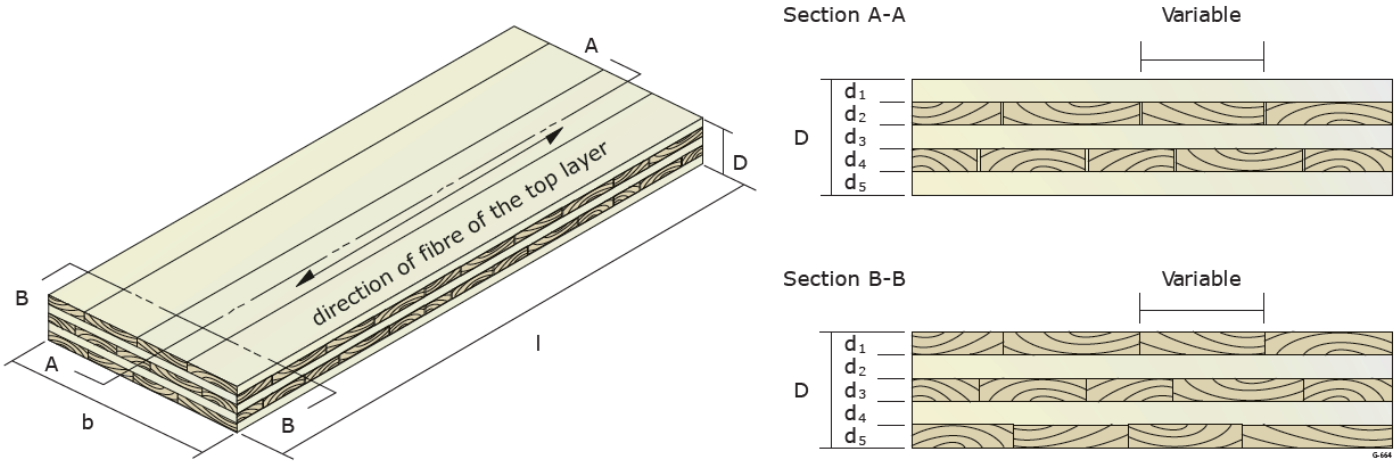

Figure 2 Example of the cross laminated panel (Gagnon & Pirvu (2011))

Several different methods for determining mechanical properties of CLT members have been developed. Some of these methods are experimental, but due to the large number of lay-ups and types of material used to form CLT members, analytical approaches are more favourable. These methods are based on the determination of the properties of the strength and stiffness of CLT member based on the material properties of the laminate planks that make it up.

Most common analytical approaches for analytical analysis of CLT are “Mechanically Jointed Beams Theory” (also named Gamma Method), “Composite Theory” (also named k-method) and “Shear Analogy”.

Gamma method is available in Annex B of EN 1995-1-1:2004 (E) (2004) and it is originally developed for beams (e.g. I or T beams) connected with mechanical fasteners. These stiffeners have stiffness K and are uniformly spaces at distance s along the length of the beam. Stiffness properties of the mechanically jointed beams are defined using the effective bending stiffness (EI_{eff}) that depends on the section properties of the beam and the connection efficiency factor γ. Factor γ is the function of the slip characteristics of the fasteners, is equal to zero for no mechanical connection and one for rigidly connected (glued) beams, and is calculated according the following equation:

$$\gamma_i = [1 + \frac{\pi^2 E_i A_i s_i}{K_i L^2}]^{-1} \quad (1)$$

where *i* is the layer number, E_i is the modulus of elasticity of the *i-th* layer, A_i area of the *i-th* layer, *L* span length. Effective stiffness is then calculated in the following way:

$$EI_{eff} = \sum_{i=1}^{n} (E_i I_i + \gamma_i E_i A_i a_i^2) \quad (2)$$

where $I_i$is the moment of inertia of the *i-th* layer and a_i distance from centroid of each layer to the neutral axis of the cross section.

To use Gamma Method for CLT beams few modifications have to be introduced. First is to assume that only the layers parallel to the longitudinal direction of the beam are carrying the load. To take into account rolling shear deformation of the cross layers they will be treated as "imaginary fasteners". This way the whole beam will be treated as multiple longitudinal layers which are connected with mechanical fasteners that have stiffness equal to the rolling shear stiffness of the cross layers between them. The fasteners stiffness is calculated using the following equation:

$$\frac{s_i}{K_i} = \frac{h_i}{G_r b} \quad (3)$$

where h_i is the thickness of the board layer in direction perpendicular to the action, G_r is the shear modulus perpendicular to the grain (rolling shear modulus) and *b* is the width of the panel.

Similarly to the Gamma Method, the k-method) uses an effective stiffness but in the form of composition factors which account for loading configurations and each individual layer's properties. The main assumptions are linear stress strain relationship and Bernoulli's hypothesis of plane sections. It takes into account perpendicular layers with the reduced stiffness equal $E_{90} = E_0/30$. Because the sheer deformation is not taken into account, this method is only suitable for relatively high span-to-depth ratios ($L/h \geq 30$). Composition factors are dependent on the loading case and could be found in Gagnon & Pirvu (2011).

The Shear Analogy method is according to Blass & Fellmoser (2004) the most precise CLT design method. It takes into account the shear deformation as well as the perpendicular layers. The beam is presented as two virtual beams A and B. Beam A is given the stiffness of the sum of all layers along their natural axes, while the beam B is given the "Steiner" part of flexural rigidity as well as the flexible sheer strength of the panel.

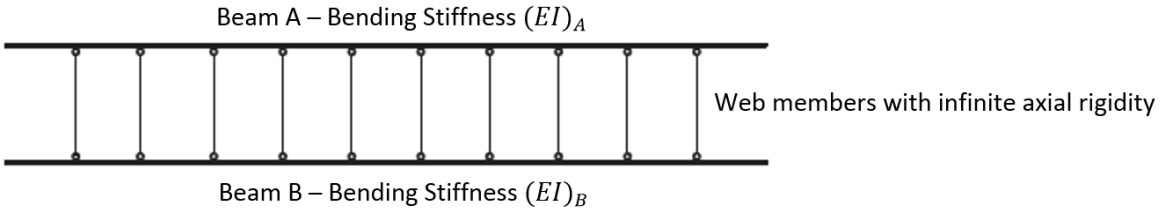

The stiffness of the beam is calculated in the following way:

$$(EI)_A = \sum_{i=1}^{n} E_i \cdot I_i = \sum_{i=1}^{n} E_i \cdot b_i \cdot \frac{h_i}{12} \quad (4)$$

$$(EI)_B = \sum_{i=1}^{n} E_i \cdot A_i \cdot z_i^2 \quad (5)$$

$$(EI)_{eff} = (EI)_A + (EI)_B \quad (6)$$

where *i* is the layer number, E_i is the modulus of elasticity of the *i-th* layer, b_i width of the *i-th* layer, h_i thickness of the *i-th* layer, A_i area of the *i-th* layer and z_i the distance from the centroid of the *i-th* layer to the neutral axis. Modulus of elasticity for the perpendicular layers is purposed to be taken as the reduced modulus of elasticity in the longitudinal direction ($E_{90} = E_0/30$).

CLT design for fire conditions is based on predictability the uniform charring rate of timber exposed the to a standard furnace fire. This is important because it is assumed that charred layer does not have any structural capacity. In addition, understanding how the increase in temperature beyond the pyrolysis front into the virgin timber affects the degradation in material properties is necessary. . Most standards calculate charring rates in similar ways but the change in material properties in the heated (but uncharred) timber is calculated differently depending on the code. One of the most important mechanical parameters is modulus of elasticity and in order to better define behaviour of timber in fire conditions, its dependence of temperature is needed to be studied in more details.

1.3 Mechanical properties of timber

Dry wood is consisted out of three main building blocks: cellulose (40-50%), hemicellulose (21-35%) and lignin (22-34%) (Drysdale (2011)). Cellulose is made up from long linear carbon chains, it makes up the cell walls, and it is very important for the behaviour of the wood, For example the tensile strength of wood is mostly provided by cellulose. Hemicellulose grows around cellulose and is essentially quite similar to it. It serves as an interface between cellulose and lignin. Lignin is considered as being the glue/cement of wood and it gives rigidity to wood. The compressive and shear strength of wood is provided by lignin (Kollmann & Cote (1968)). Beside these three main component, wood is also consisted out of small organic compounds, extractives.

When considering defining properties of wood it is not as simple task as just considering properties of these three polymers in isolation. Wood properties are defined also by other factors such as species, age, moisture content, environmental factors position of localised defects etc.

Generally, tree species are classified as being port of one of two major classes, hardwoods and softwoods. Most hardwoods have broad leaves and shed them at the end of each growing season. This is in contrast with softwoods for which most species are evergreen.

When observing a tree log, three zones can be distinct, bark, sapwood just beneath it and the central zone, heartwood. Sapwoods purpose is to allow sap conduction and food storage. As the tree grows older sapwood zone shrinks and gets replaced with more durable heartwood due to the formation of sap deposits in the cells. However once dry there is no consistent difference between heartwood and sapwood in weight or strength. Inside the growing rings of wood two zones can be identified, early growing springwood and late growing summerwood. Summerwood has more solid wood substances than springwood, this can have an important effect on the properties of wood.

Water in the wood can be contained in two forms, either like “free water” in the cavities between cells or as “absorbed water” in the capillaries of the cells. When wood starts losing moisture, first the free water is evaporated and then the loss of the absorbed water follows. The point when all of the free water has evaporated is called fibre saturation point and for post of the wood species is around 25-30% of moisture. Increase of moisture above this point has no significant effect on mechanical properties of wood, but as the moisture level drops below fibre saturation point, in general, wood starts to shrink and strength increases.

The moisture content also changes with temperature and time. As a piece of wood is heated, the moisture is evaporated, some of this moisture is lost, but most is driven further into the wood. This moisture then condenses, increasing the moisture content at that point, often up to the fibre saturation point for many species of timber. Wood strength and stiffness decreases with increasing moisture content (up to the fibre saturation point). That means that at the fibre saturation point the strength and stiffness of wood is a minimum as a function of moisture content. This shows that elevated temperature has a complex effect on the mechanical properties of wood as it does not only influence the material itself but also the moisture transport inside of it that also has a strong influence on the mechanical properties.

Thomas (1996) mentions the problems with measuring material properties at elevated temperatures. Measuring the material properties of the piece of timber at elevated temperature and moisture is not difficult in theory, but in practice it is very difficult to ensure

that the timber is at the same moisture content and temperature throughout. Temperature can be measured with thermocouples, even though they can affect mechanical and thermal properties but the moisture content is more difficult to maintain or measure. Even if these measuring and maintaining problems were easier to overcome the problem of scale is present. It is hard to predict the behaviour of the correlation between the results obtained on the relatively small samples and local behaviours of large specimens such as floor and wall systems. The combination of these effects may be more or less severe than simple addition or multiplication of the effects would suggest.

EN 1995-1-2:2004 (E) (2004) uses the modulus of elasticity dependence of the temperature based on the tests by König (2000). In that study, the samples were heated on the bottom side only and mechanical properties were calculated based on the observed sample responses. Since these are not direct measurements, the results are effective parameters specific to the test setup used, rather than directly measured material properties.

Thomas (1996) investigated the effects of the assumed modulus of elasticity dependence of temperature on the model predictions. Model used tensile elastic modulus data, with all elements at temperatures above 300°C assumed to have zero strength and stiffness. He based his model on the same principles as König (1991) and used the test results from König (1994), but only calculated the elastic modulus at failure. Two methods gave similar results for compressive modulus of elasticity, but for the tensile one results differ significantly.

In Östman (1985) test have been done to determine the wood mechanical properties at temperatures and moisture contents simulating fire conditions. Test samples were small scale wooden planks with thickness of around 1 mm in order to achieve constant temperature gradient and a rapid temperature equilibrium. To achieve constant moisture content wood specimens were submerged in silicone oil in order to obtain stable moisture conditions. The samples were tested trough the tensile loading and modulus of elasticity was determined from the initial linear part of the stress-strain curves. It concluded that an increase in temperature leads to a more or less linear decrease in the in the modulus of elasticity up to about 200°C and that above 200°C there is a more rapid decrease due to thermal softening.

In Gerhards (1982), gives a summary of at that time available information on the effect of moisture content and temperature on mechanical properties. Based on the available data it

shows that at moisture content of approximately 12% the temperature has little effect on the modulus of elasticity until the temperatures of approximately 200°C after which it starts to decline faster with increasing temperature. He also mentions great effect moisture has on the modulus of elasticity. Gerhards (1982) showed that modulus of elasticity of timber at 20°C drops for approximately 20% from no moisture to the fibre saturation point.

E. Schaffer (1971) among other examined the decrease of the modulus of elasticity of wood at elevated temperatures and concluded that a linear expression is the best to fit the initial temperature effect on the modulus and that a significant decrease in the modulus only occurred when the temperatures exceeded 140° C. He also references work by James (1961) who measured reduction of the dynamic modulus of elasticity and concluded that it drops linearly until the temperature of 100°C.

Kollmann (1951) has found that modulus of elasticity of pine in compression decreases for approximately 33% for at 100°C. E. Schaffer (1986) tested glulam timber beams and reported that modulus of elasticity parallel to the grain does not reduce significantly until 180°C, approximately 12%, after which it linearly decreases to zero at 300°C. Glos & Henrici (1991) conducted tests on structural timber of sizes used in practice in bending, compression and tension. For tension and bending, for timber with an initial moisture content between 7 and 10 percent, at 100°C the modulus of elasticity has decreased to 88 percent of its initial value in tension, and to 75 percent in bending.

H White, Cramer, & Shrestha (1993) examined the behaviour of Metal-Plate-Connected wood truss in fire conditions. To model that behaviour they measured the loss of tensile stiffness of the Southern Pine 5x10 cm samples when exposed to a constant elevated temperature for 30 to 60 min. Results show that relative modulus of elasticity is constant for the temperatures up to 100°C and then almost linearly drops to 0.4 at 250°C.

Young & Clancy (2001) inspected mechanical compression properties of wood at temperatures simulating fire conditions. They tested mechanical properties of moist (12%) and dry samples to determine mechanical properties. Sample dimensions were 90 x 35 x 300 mm and uniform temperature was assumed. Some trends were noticed: first modulus of elasticity of dry samples would have almost no decrease towards 100°C, gradually decrease until 200°C and decrease more steeply at higher temperatures. For the moist samples,

decrease of modulus of elasticity was much more intense until 100°C after which the authors assumed same behaviour as dry samples.

Jong & Clancy (2004) continued the previous research and tried to take into an account the stress and creep during the previous tests for explaining the behaviour of the modulus of elasticity at elevated temperatures. Their results support the results of previous research, but also still suffers similar limitations. The model they proposed is applicable to light-timber framed structures that experience similar histories of temperature, moisture content and stress as the specimens in the experiments. The authors suggest a more rigorous detailed model, which incorporates the variable of time explicitly

They showed that creep had an evident effect on the measurements of modulus of elasticity. Creep caused by the elevated temperature, moisture transfer and stress applied on the specimen influenced the measured strain and that way calculated modulus of elasticity. This prevented determination of the independent influence of temperature on modulus of elasticity.

At elevated temperatures and high moisture content creep deformations increase dramatically as referenced by Schaffer (1986). This effect is important as the moisture content of more than 20% occurs at the parts of the cross section with temperatures approaching 100°C as mentioned by White & Schaffer (1981). It should be noted that mechano-sorptive creep can also have an important role when the timber starts to dry out as mentioned König (2000). There it is also referenced that steam has no influence on creep.

All of the information of the behaviour of the modulus of elasticity of timber at elevated temperature found in literature has been presented in Figure 3.

In order to analyse this behaviour without the added influence such as creep etc. a novel testing method using the modal analysis is purposed.

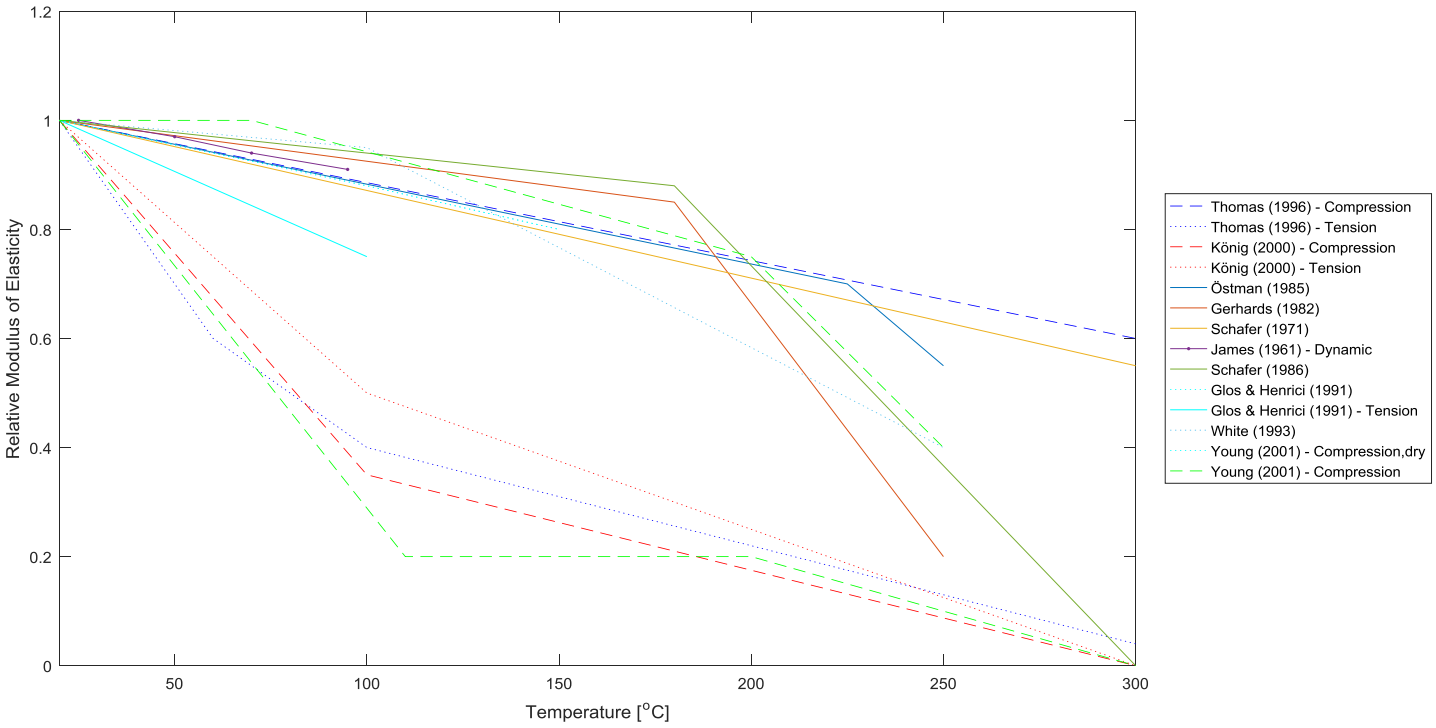

Figure 3 Different functions of reduction of modulus of elasticity of timber with elevated temperature found in literature

1.4 Modal analysis

In this study modal analysis will be used as a tool for determining stiffness of the system. Modal analysis is defined as the study of the dynamic characteristics of a mechanical structure in the frequency domain. It is based on the fact that all real systems have multiple numbers of frequencies that they tend to oscillate in the absence of any driving or damping force, called natural frequency or eigenfrequency. It will be demonstrated on the simple case of the system with single degree of freedom. Real systems have multiple degrees of freedom, but they can generally be represented as a superposition of single degree of freedom models.

Figure 4 shows discrete parameter model of the single degree of freedom system. It is consisted of the mass connected with an elastic spring to a static boundary. It is also connected to a viscoelastic damper. When it is excited with an external force, its movement can be characterized with the following equation:

$$m\ddot{x} + c\dot{x} + kx = f(t) \tag{7}$$

where m is the mass, $k$is the stiffness of the spring, c is the damping constant and $f(t)$ is the exciting force. By dividing the equation (7) with mass m and setting $f(t) = 0$ for free vibrations, new form is gained:

$$\ddot{x} + 2\zeta\omega_n\dot{x} + {\omega_n}^2 x = 0 \tag{8}$$

where $\omega_n = \sqrt{k/m}$ is the natural circular frequency, $\zeta = c/(2m\omega_n)$ is the damping ratio.

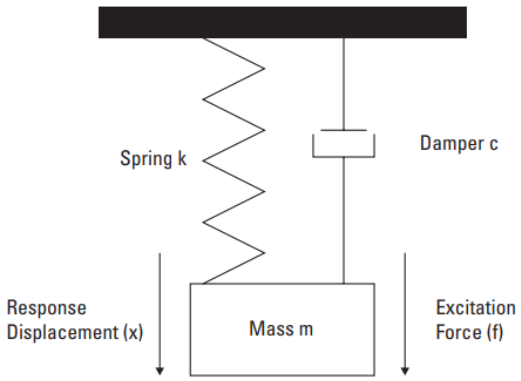

*Figure 4 Discrete parameter model of the single degree of freedom system (*Agilent Technologies (2000)*)*

The solution of this equation is a sinusoid with exponentially decaying amplitudes defined with the equation (9) presented at Figure 5. Natural circular frequency has units of rad/s, but typically it can also presented as natural frequency $f_n = \omega_n/(2\pi)$ in Hertz (Hz).

$$x(t) = e^{-\zeta\omega_n t}\left[x(0)\cos\omega_D t + \left(\frac{\dot{u}(0) + \zeta\omega_n x(0)}{\omega_D}\right)\sin\omega_D t\right] \tag{9}$$

where $\omega_D = \omega_n\sqrt{1-\zeta^2}$ presents damped natural frequency.

This shows the behaviour of the system when no external forces acting on it. When the external force excites the system, equation (7) has different solution. For a special case of the impulse load, which represents a very large force that acts for an infinitely short time but with a time integral that is finite, solution of the equation (7) looks like this:

$$x(t) = \frac{1}{m\omega_D}e^{-\zeta\omega_n t}\sin\omega_D t \tag{10}$$

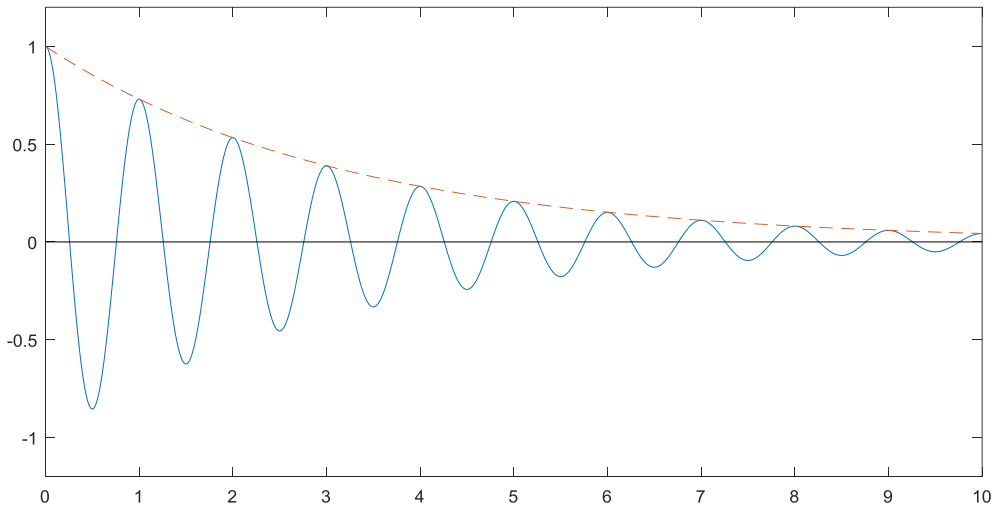

Figure 5 Free vibrations of the damped single degree of freedom system

As mentioned before real systems have multiple degrees of freedom but their behaviour can be described as superposition of multiple singe degrees of freedom systems. Next, the system of the simply supported beam with will be analysed.

We consider the Euler-Bernoulli beam. The transverse displacement at any point x and time t is denoted by $y(x,t)$ and transverse force per unit length by $f(x,t)$. The system parameters are the mass per unit length $m'(x)$ and bending stiffness $EI(x)$. Consideration of the equilibrium of the forces and moments yields the following governing differential equation of motion.

$$\frac{\partial^2}{\partial x^2}\left(EI(x)\frac{\partial^2 y}{\partial x^2}\right) + m'(x)\frac{\partial^2 y}{\partial t^2} = f(x,t) \tag{11}$$

The natural frequencies and mode shapes are obtained considering the homogeneous solution of the beam vibration equation. Undammed mode in bending vibration of the beam with uniform sectional property are considered. For free vibration $f(x,t) = 0$ and assumption is that the response is given by:

$$y(x,t) = \phi(x)\sin\omega_n t \tag{12}$$

When substituted in the equation (11) the following form is obtained:

$$\frac{\partial^4 \phi}{\partial x^4} - a^4 \phi(x) = 0 \qquad (13)$$

where $a^4 = m{\omega_n}^2/EI$

Solution of equation (13) is:

$$\phi(x) = A \sin ax + B \cos ax + C \sinh ax + D \cosh ax \qquad (14)$$

where A, B, C and D are integration constants determined from the boundary conditions for the simple beam:

$$\phi(0) = \phi(L) = 0 \text{ and } \phi"(0) = \phi"(L) = 0$$

That leads to $A \sin aL = 0$, which if we exclude the trivial solution $(A = 0)$ gives solution

$a_n L = n\pi, n = 1,2, \ldots$ and finally:

$$\omega_n = (n\pi)^2 \sqrt{\frac{EI}{m'L^4}} \qquad (15)$$

This way a relationship between the oscillation of the simply supported beam and its bending stiffness has been derived. It should be noted that based on equations (10) and (15) frequency of the oscillation of the simply supported beam only depends on mechanical and geometrical characteristics of the beam, not on the intensity of the impulse force.

When excitation is applied, the equation of motion leads to the frequency response of the system. The frequency response is a complex quantity and contains both real and imaginary parts (rectangular coordinates). It can be presented in polar coordinates as magnitude and phase, as well. Frequency response function has complex quantity and as such cannot be properly presented on the single two-dimensional plot. Even though motion of the system has been previously described by its displacement $\big(y(x,t)\big)$ for the frequency response function, velocity and acceleration could also be used as response variable, with the notion that acceleration is currently the accepted method of measuring modal response.

One of the usual methods of presenting frequency response function is to plot the polar coordinates, magnitude and phase versus frequency. The natural frequencies of the system will be noticeable by the peak values in the magnitude plot and $\pi/2$ change in the phase plot.

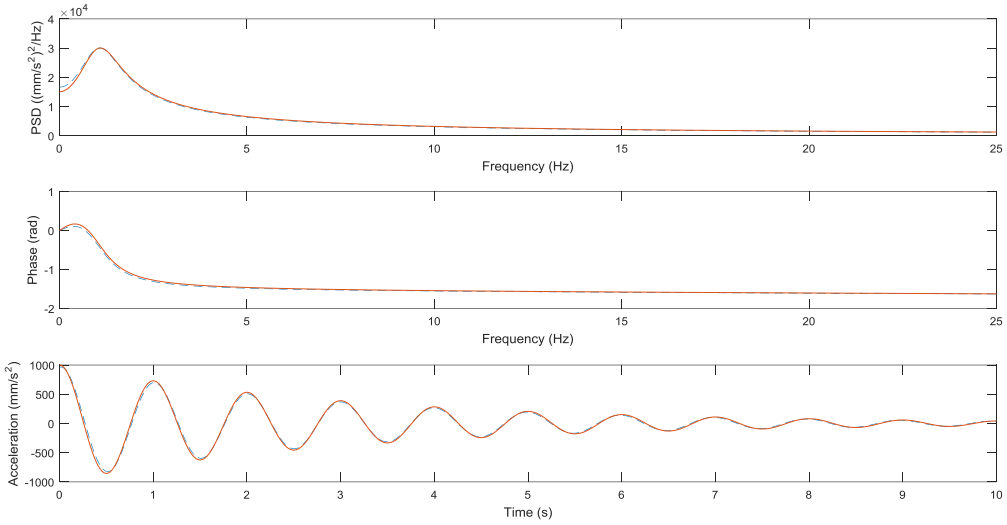

Figure 6 Example of the magnitude and phase plots for the acceleration of the single degree of freedom system

2. Method

An analysis of the influence of elevated temperatures on the modulus of elasticity of timber in this study has been conducted in two parts. First, a numerical analysis has been conducted to estimate the behaviour of the CLT beams at elevated temperatures lower than ignition temperature (300°C) based on the knowledge available in the literature. Afterwards tests on heated CLT beams were performed to investigate the real behaviour of the samples.

2.1 Thermal model

To predict the behaviour of the test specimen MATLAB (2016) program has been created. It consists of two main parts, thermal and stiffness model. In this chapter, thermal model will be explained. For any control volume, conservation of energy is represented by the following equation:

$$\dot{E}_{in} - \dot{E}_{out} + \dot{E}_{gen} = \dot{E}_{sto} \tag{16}$$

where $\dot{E}_{in}$ is the energy in, $\dot{E}_{out}$ is the energy out, $\dot{E}_{gen}$ is the energy generated, and $\dot{E}_{sto}$ is the energy stored. Because the temperature range observed in this study is lower than ignition temperature of wood the energy generated term is neglected. Based on this Fourier's heat transfer equation (17) needed to be solved.

$$\frac{\partial}{\partial x}\left(k_x \frac{\partial T}{\partial x}\right) + \frac{\partial}{\partial y}\left(k_y \frac{\partial T}{\partial y}\right) + \frac{\partial}{\partial z}\left(k_z \frac{\partial T}{\partial z}\right) = \rho c_p \frac{\partial T}{\partial t} \tag{17}$$

where $k_{x,y,z}$ is thermal conductivity in given direction, ρ is the density and c_p is the specific heat. It was assumed that due to the heating conditions in the tests the distribution of temperature along the longitudinal axis of the beam is uniform so the 2D analysis of the temperature distribution across the cross section was used and equation (17) becomes:

$$\frac{\partial}{\partial x}\left(k_x \frac{\partial T}{\partial x}\right) + \frac{\partial}{\partial y}\left(k_y \frac{\partial T}{\partial y}\right) = \rho c_p \frac{\partial T}{\partial t} \tag{18}$$

For the transient heating conditions equation (18) has no analytical solution so it was solved numerically using the finite difference method with explicit numerical scheme. In essence,

the whole cross section is divided in finite numbers of cells each with its own temperature. In addition, the simulation time has been divided in the finite number of time steps. For each time step and cell temperature is calculated based on the temperature of its and neighbouring cells in the previous time step schematically presented on Figure 7.

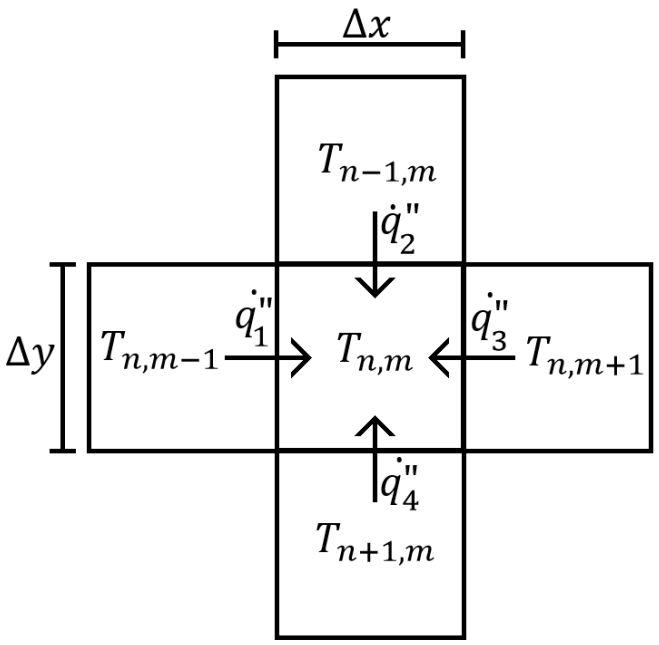

$$\dot{q}''_1 = \frac{k_x}{\Delta x}(T_{n,m-1} - T_{n,m})$$

$$\dot{q}''_2 = \frac{k_y}{\Delta y}(T_{n-1,m} - T_{n,m})$$

$$\dot{q}''_3 = \frac{k_x}{\Delta x}(T_{n,m+1} - T_{n,m})$$

$$\dot{q}''_4 = \frac{k_y}{\Delta y}(T_{n+1,m} - T_{n,m})$$

Figure 7 Graphical representation of the thermal models calculation process

Grid size was chosen to be uniform in both *x* and *y* direction and equal to 1mm. This size is the result of multiple criteria, small enough to provide grid size independent solution and provide adequate resolution for later calculation of the stiffness of the cross section and big enough to enable fast computation.

Values reported in the literature for the thermal properties of wood exhibit wide variability. Benichou (1999) has collected different values of thermal properties of timber available in the literature. Multiple functions of thermal properties were used in this study in order to get the best prediction of the temperature gradient inside of the beam.

First thermal properties used in the model were based on the values for timber given in EN 1995-1-2:2004 (E) (2004). And it was based on the previously mentioned research by König (2000). The values are presented in Table 3.

Table 3 Thermal properties of timber from EN 1995-1-2:2004 (E) (2004)

Temperature [°C]	Thermal conductivity [W/(m·K)]	Specific heat [J/(kg·K)]	Ratio of density to dry density*
20	0.120	1530	1+ω
99	0.133	1770	1+ω
99	0.133	13600	1+ω
120	0.137	13500	1.00
120	0.137	2120	1.00
200	0.150	2000	1.00
250	0.123	1620	0.93
300	0.097	710	0.76
350	0.070	850	0.52
400	0.077	1000	0.38
600	0.177	1400	0.28
800	0.350	1650	0.26
1200	1.500	1650	0.00

** ω is the moisture content*

Next thermal properties values used were based on the research of Janssens (2004). He developed model to evaluate the charring rate of wood. It was intended to keep the model simple and it accounts for the four major factors that affect the thermal degradation of wood: dry density of the wood; moisture content of the wood; lignin content of the wood; char contraction. The predictive capability of the model was evaluated based on ASTM E 119 furnace data obtained for a Douglas fir glulam beam tested under different loads. Its predictions, with some adjustment for moisture effects, are in reasonable agreement with the measurements. Author states that the model should be used to predict performance of wood members exposed under thermal conditions that are similar to the standard fire. The values are presented in Table 4.

Table 4 Thermal properties of timber from Janssens (2004)

Temperature [°C]	Thermal conductivity [W/(m·K)]	Specific heat [J/(kg·K)]	Ratio of density to dry density*
20	0.130	1450	1+ω
100	*0.160*	*1805*	*1+ω*
120	0.130	1895	1+ω
200	*0.150*	*2250*	*1+ω*
300	0.133	760	0.74
350	*0.125*	*760*	*0.56*
400	0.133	760	0.39
600	*0.166*	*760*	*0.28*
1100	0.250	760	0.27

** ω is the moisture content*

Fredlund (1993) developed one dimensional model for both uncharred and charred portions of the cross-section, as well as the growth of the charred layer in. Functions for thermophysical properties were presented and validated based on the failure time of the specimen in the oven test. It was shown that the difference between the failure times predicted by the model and measured in the actual oven tests is not more than 10 min.

Table 5 Thermal properties of timber from Fredlund (1993)

Temperature [°C]	Thermal conductivity [W/(m·K)]	Specific heat [J/(kg·K)]	Ratio of density to dry density*
20	*0.120*	*1450*	*1+ω*
95	*0.128*	*1783*	*1+ω*
115	*0.130*	*1872*	*0.95*
200	*0.140*	*2250*	*0.95*
250	*0.145*	*1505*	*0.88*
290	*0.150*	*910*	*0.74*
300	*0.100*	*760*	*0.70*
310	*0.050*	*760*	*0.67*
400	*0.065*	*760*	*0.35*
600	*0.100*	*760*	*0.26*
1200	*0.200*	*760*	*0.23*

** ω is the moisture content*

At last the thermophysical properties defined by Knudson (1975) were used. He developed a method that is general in respect to member size, configuration, and exposure conditions to predict behavior of structural wood members both during and following fire exposure. He used finite-element method to predict the temperature in the member and then combined it with the knowledge of the effects of temperature and time on mechanical properties of material composing the member to predict structural performance. Developed structural model was able to predict strength losses for beams and columns within 8 percent of actual strength losses after various periods of exposure to different standard fires.

Table 6 Thermal properties of timber from Knudson (1975)

Temperature [°C]	Thermal conductivity [W/(m·K)]	Specific heat [kJ/(kg·K)]	Ratio of density to dry density*
20	*0.125*	*1450*	*1+ω*
90	*0.146*	*1475*	*1+0.90ω*
100	*0.149*	*10000*	*1+0.89ω*
110	*0.153*	*2200*	*1+0.88ω*
190	*0.177*	*2175*	*1+0.76ω*
200	*0.180*	*675*	*1+0.75ω*
280	*0.130*	*683*	*0.82*
300	*0.117*	*685*	*0.7*
350	*0.086*	*689*	*0.27*
400	*0.093*	*694*	*0.26*
500	*0.106*	*703*	*0.24*
800	*0.146*	*729*	*0.18*
1200	*0.200*	*765*	*0.18*

** ω is the moisture content*

All of thermal properties mentioned are also graphically presented on Figure 8Figure 10.

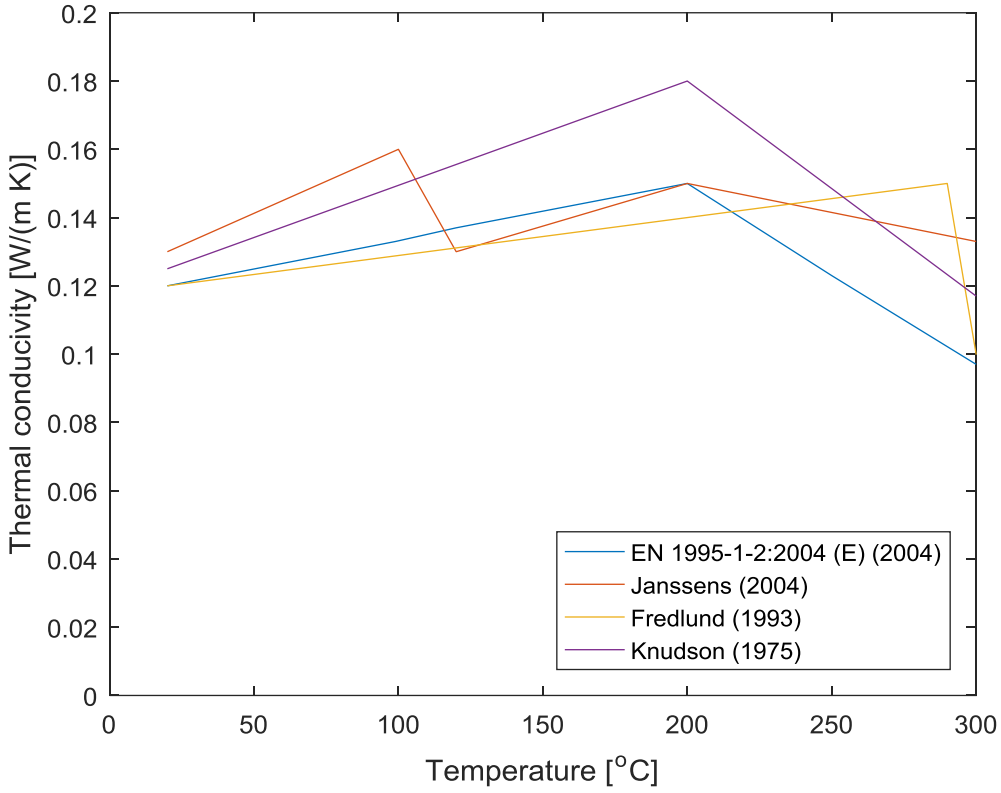

Figure 8 Temperature-thermal conductivity relationship for wood

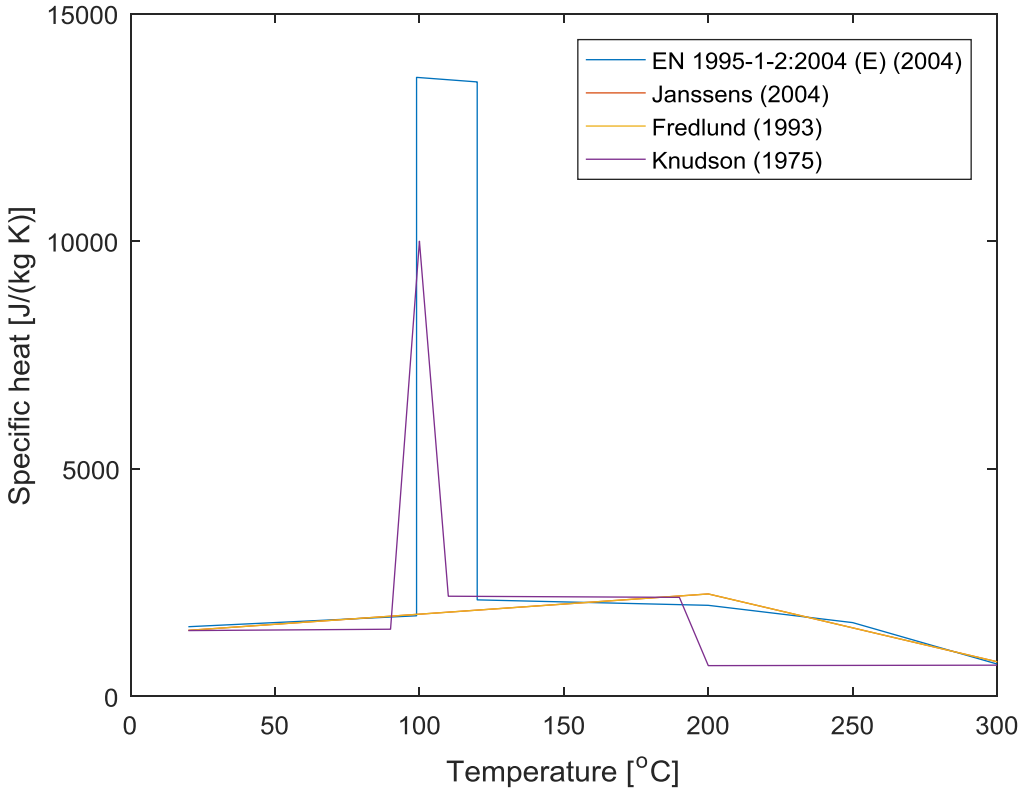

Figure 9 Temperature-specific heat relationship for wood

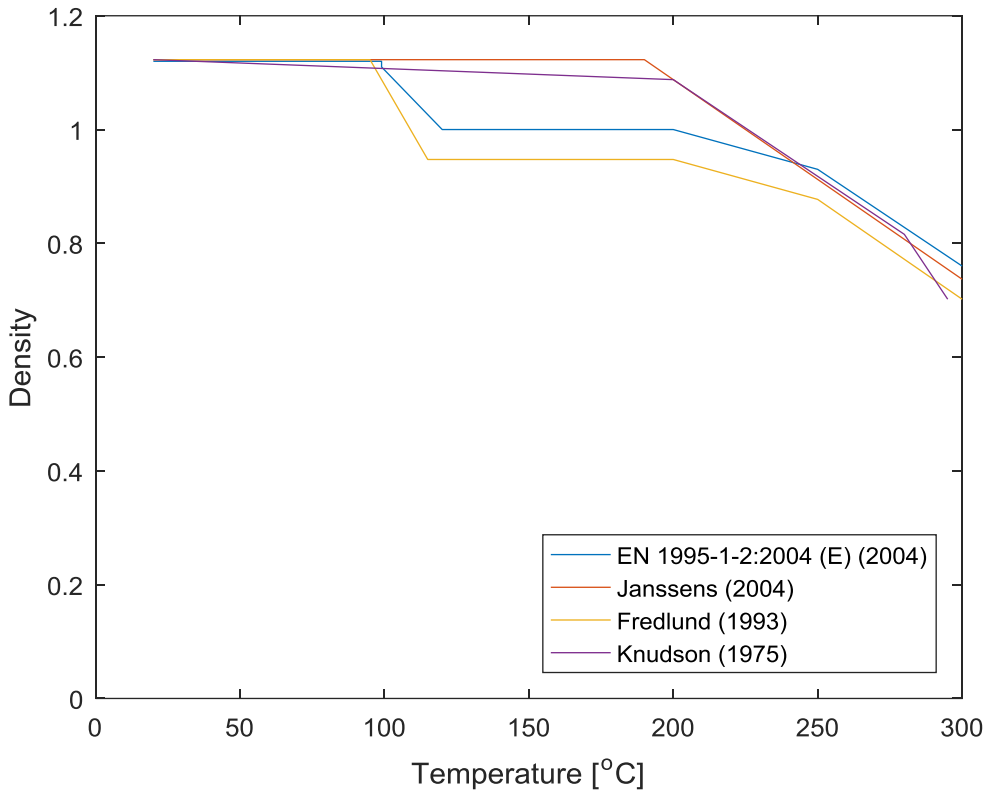

Figure 10 Temperature-density ratio relationship for softwood with an initial moisture content of 12 %

Boundary conditions were presumed to be constant on all edges of the cross section, this coupled with the fact that cross section of the tested beams had two orthogonal axes of symmetry made it possible to use symmetric boundary conditions. This means that in order to save memory and computing time, only one quadrant of the cross section was analysed (Figure 11). On the inside edges of the quadrant boundary condition was that there is no energy transfer, as when looking at the whole cross section the neighbouring cells would have the same temperature due to the symmetric heating conditions. On the outer edges of the quadrant, boundary conditions were based on the sum of the convective and radiative heat transfer from the surrounding hot air. Emissivity was chosen as 0.8 based on the recommendations form Eurocode. As for the connective heat transfer coefficient was not taken per Eurocode because the heating conditions inside the heating chamber used for tests were not the same as for the oven test for which the Eurocode connective heat transfer coefficient prescribed. Instead, because the heating chamber used for the tests is unique, the convective heat

transfer coefficient was chosen manually to best fit the results obtained from the heating tests.

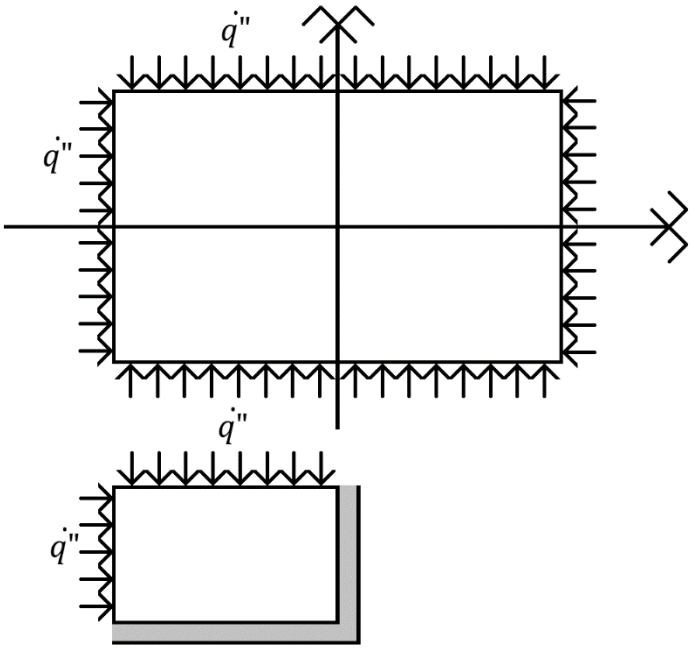

Figure 11 Use of symmetry of cross section and heating conditions

Because of the characteristics anisotropic characteristics of wood as the material heat conduction coefficient is not equal in all directions. More precisely, conductivity along the grain has been reported as greater than conductivity across the grain by a factor of 1.5 to 2.8, with an average of about 1.8 (Ross & USDA Forest Service. (2010)). Even though in this model only the cross section thermal gradient has been analysed, because of the defining characteristic of CLT conduction coefficient of the perpendicular layers in the horizontal direction had to be multiplied with 1.8.

2.2 Stiffness model

As mentioned in Chapter 1.2 there are multiple ways of designing CLT beams and determining stiffness which produce similar end results (Gagnon & Pirvu (2011)). To numerically determine the stiffness of the CLT beams at elevated temperatures in this study modified "Shear analogy" method has been chosen. The modification was needed to take into account the thermal gradient and as its consequence, unequally distributed modulus of elasticity across the cross section. This was done in the following way.

In most cases, bending stiffness of the cross section in the *y* direction is defined as the product of modulus of elasticity *E* and moment of inertia in the y direction I_y. That is done under assumption that the modulus of elasticity is evenly distributed across the whole cross section. As mentioned earlier, this is not the case for CLT even at ambient temperatures because of the lower modulus of elasticity of perpendicular layers and this causes the need for previously mentioned methods for designing CLT beams. With elevated temperatures, due to thermal gradient across the cross section and reduction of modulus of elasticity due to it, modulus of elasticity distribution becomes even more uneven. For these cases the bending stiffness of the cross section in the y direction has to be defined in the following way:

$$(EI)_{eff} = \iint_A E(x, y, T) \cdot y^2 dA \tag{19}$$

where $(EI)_{eff}$ is the bending stiffness of the cross section in the y direction, y is the distance from the neutral axis and A is the area of the cross section. Because of the complexity of thermal gradient this equation has to be solved numerically.

This was done in the following way. First, the whole cross section is divided in the 1 x 1mm grid, same as the grid used for the thermal model. Then the position of the neutral axis has to be calculated. Even though for pure bending it goes through the centroid of the cross section, because of the different reduction of modulus of elasticity of wood in compression and tension with elevated temperature it changes its position. Location of the neutral axis is calculated in a way that first it is assumed that it is positioned in the middle of the cross section. One half is assumed to be compressed and other tensioned. Based on the

temperature gradient obtained from the thermal model, reduced modulus of elasticity of each cell is determined. For that distribution of modulus of elasticity new position of the neutral axis is calculated. Which cells are compressed and which are tensioned is determined based on the new neutral axis position and new distribution of modulus of elasticity is obtained. From that distribution, position of the neutral axis is again calculated. This process is repeated until the difference of the two successive neutral axis positions is less than 1%.

With the final position of the neutral axis determined the bending stiffness of the cross section can be calculated based on the equation (19). For each cell, modulus of elasticity is determined based on the temperature and whether it is in the compression or tension zone. Than its contribution to the bending stiffness is calculated using the Steiner's theorem:

$$\Delta EI(x, y, T) = \frac{1}{12} \cdot E(T) \cdot \Delta x \cdot \Delta y^3 + E(T) \cdot \Delta x \cdot \Delta y \cdot y^2 \tag{20}$$

where Δx and Δy are cell dimensions, $E(T)$ is the reduced modulus of elasticity and y is the distance from the neutral axis. The bending stiffness of the whole cross section is calculated by summing up all of the cell contributions.

$$(EI)_{eff} = \sum \Delta EI(x, y, T) \tag{21}$$

2.3 Experimental testing

After the numerical model of the behaviour of the CLT beam at elevated temperatures created based on the knowledge found in literature second part of this study is to try to experimentally validate it. This was done using the modal analysis of the heated simply supported CLT beams.

Four sample beams were tested with their characteristics presented in the Table 7. All test beams had same dimensions, length of 3 m, height of 100 mm and width of 300 mm width density of 450 kg/m³.

Table 7 Characteristics of the test CLT beams

n	Number of layers	Height of layers [mm]	Glue
Test 1	5	20 – 20 – 20 – 20 – 20	melamine-urea formaldehyde
Test 2	3	40 – 20 – 40	melamine-urea formaldehyde
Test 3	3	40 – 20 – 40	melamine-urea formaldehyde
Test 4	5	20 – 20 – 20 – 20 – 20	Poly-Uterine

Figure 12 CLT beams used for experiments

Beams were tested in the special heating chamber O-105. The chamber is 4 m long, 50 cm wide and 110 cm tall. It is made of wood with its walls protected with 5 cm thick insulation. The top of the chamber consists of four removable lids made of the same material as the walls. On the left side of the chamber two windows are positioned, one on each side, which provide monitoring of the samples during the tests. Inside of it, two simple supports are positioned with the distance of 2.7 m between them.

In the upper part of the chamber, heating system is positioned. It is consisted out of tubing system that can provide inflow of the air at the both sites of the chamber. At each inlet at both sides, a heater is located. It is externally controlled to be able to achieve desired steady temperature. Tubing system is connected with external fan that provides constant and steady air inflow during the tests. Fan is constantly active during the tests with the activity of the heater being conditioned with the temperature inside the chamber measured by the thermocouple.

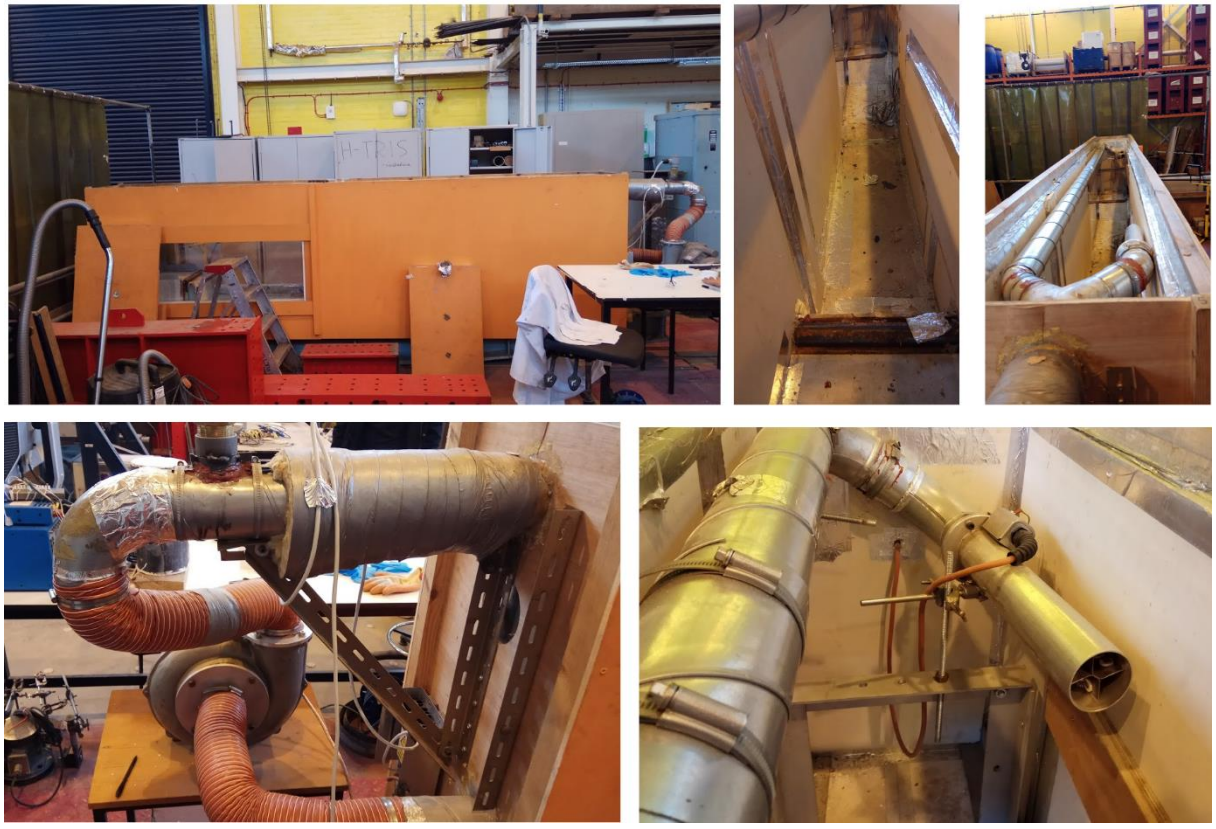

Figure 13 Heating compartment used for the experiments showing outsides, insides, heating system and fan used

The heating chamber was not deemed able to withstand and maintain temperatures higher than 150°C. For those reasons during the tests steady temperature of 140°C was chosen. In

practice, this means that heater was active until the temperature inside of the chamber achieves the targeted value. At that point, the heater would automatically deactivate until the temperature dropped under 140°C when it would activate again and so on.

All beams were fitted with the seven 1.5 mm diameter Type-K Inconel sheathed thermocouples to measure the temperature gradient progression during the tests. They were inserted from the top side of the beam and were positioned the same way for all test beams as presented on Figure 14. Exact position of the thermocouples was chosen based on the results from numerical model and to get the best good representation of the thermal gradient trough the beam needed for validation of the numerical model.

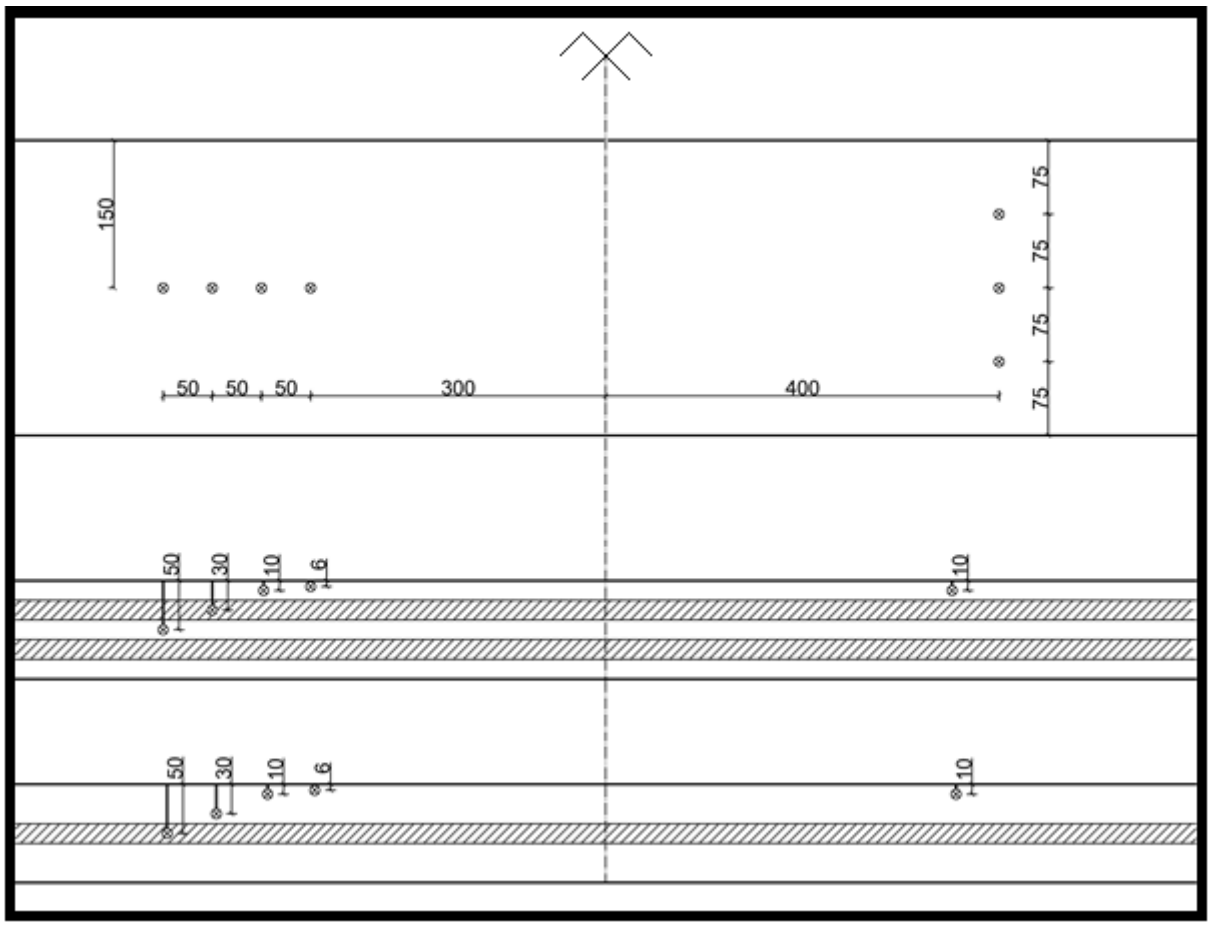

Figure 14 Thermocouple positions in sample beams

For modal analysis, charge output triaxial accelerometer with UHT-12™ element for environments up to +480°C and 3.2 pC/g sensitivity was used. This charge mode accelerometer outputs a strong, highimpedance charge signal directly from their sensing element. It does not contain built-in signal conditioning electronics so the signal is conditioned

externally by in-line charge converter prior to being analysed by a readout or recording device. In this case, In-line charge converter with 10 mV/pC sensitivity specially made for high temperature sensors was used. The connection to the in-line charger was made using 3 m long hardline mineral insulated coaxial cables. The absence of built-in electronics permits operation to elevated temperatures of up to 480 °C and extreme application up to 650 °C.

For data logging, accelerometer trough the in-line charger was connected to the National Instruments CompactDAQ-9174 chassis fitted with the The NI 9230 is a 3-channel C Series dynamic signal acquisition module for making industrial measurements from integrated electronic piezoelectric (IEPE) and non-IEPE sensors. Chassis was connected to a laptop which collected acceleration data using LabVIEW (2018) software.

The accelerometer was positioned in the middle of the span on the top side of the beam, this spot was chosen because the deflections are maximal at that point and that will produce bigger accuracy of the measured signal.

The tests were performed in the following order. First the beam would be placed in the heating chamber and the thermocouples and the high-temperature accelerometer would be placed. Than the beam would be hit in order to excite it and the accelerometer response would be measured. The beam would be hit at least three times in order to get more accurate measure of the oscillating frequency at that moment. After the oscillating response was recorded for the ambient conditions the fan and heater inside the chamber are started and the beam starts to heat up. Every time the temperature at 6 mm thermocouple would rise for 10°C beam would be excited at least three times. This was done until the temperature would achieve 90°C and afterwards, until 110°C the interval would be 5°C. At that point the temperature rise would be much slower so the beam would be excited approximately every 15-20 min.

3. Results and Discussion

3.1 Thermal model

In this study thermal model of CLT cross section was developed based on thermal properties gathered from four different sources: EN 1995-1-2:2004 (E) (2004), Janssens (2004), Fredlund (1993) and Knudson (1975). Figure 15 shows an example of the model's output temperature gradient. Model was validated using the temperature data recorded during the heating of the four CLT beams.

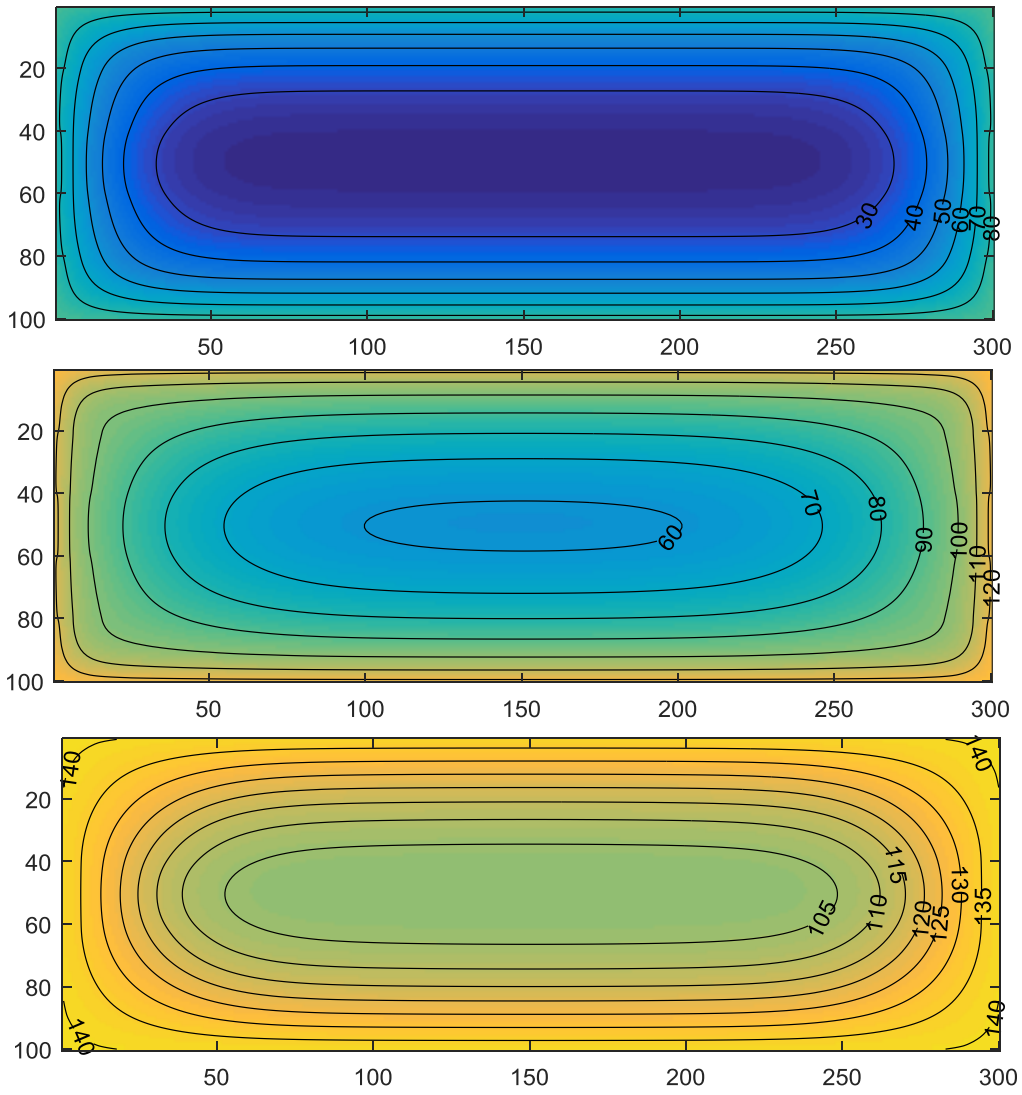

Figure 15 Modeled temperature gradient of the five-layered cross section after 15, 60 and 210 min

Aside from the mentioned thermal properties and the geometry of the cross section, as the input for the model gas temperature in the heating chamber, emissivity and convective heat transfer coefficient were used. Gas temperature was taken directly from the data recorded from the thermocouple inside the heating chamber. Emissivity was inputted as $\varepsilon = 0.8$ based on the recommendations from EN 1991-1-2:2004 (E) (2004). The convective heat transfer coefficient was determined manually to best fit the temperature data close to the edge of the cross section as the heating chamber and the airflow conditions inside of it were unique and no literature value could be easily accepted.

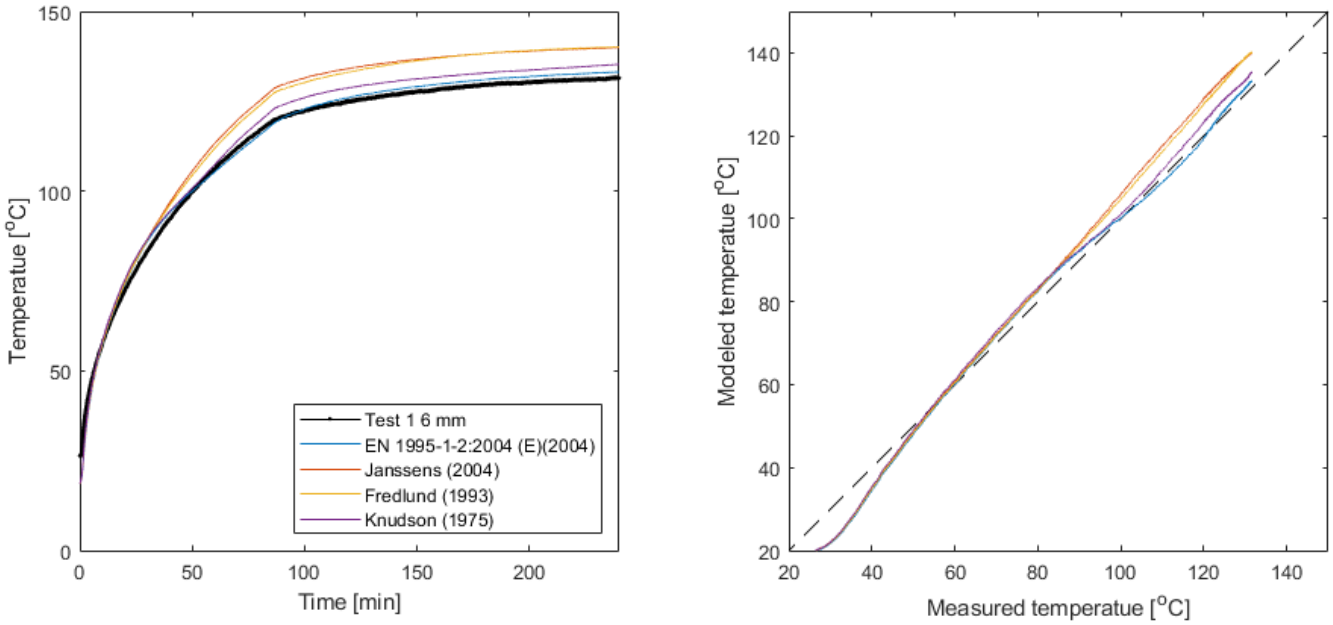

Figure 16 Comparison of the temperatures at 6 mm under the surface of the beam measured during Test 1 and those predicted by the model using different thermal properties

Figure 16 presents the temperature trough time recorded with the thermocouple positioned at 6 mm under the surface of the beam and temperatures at the same position predicted by the thermal model. It can be noted that when using thermal properties provided by Janssens (2004) and Fredlund (1993) temperature is overpredicted. When thermal properties by Knudson (1975) are used the results are closer the measured ones but thermal properties by EN 1995-1-2:2004 (E) (2004) present the best prediction. On the right side of the Figure 16 direct comparison was presented and it can be seen deviation of the model from the measured values deviates less with longer time of heating.

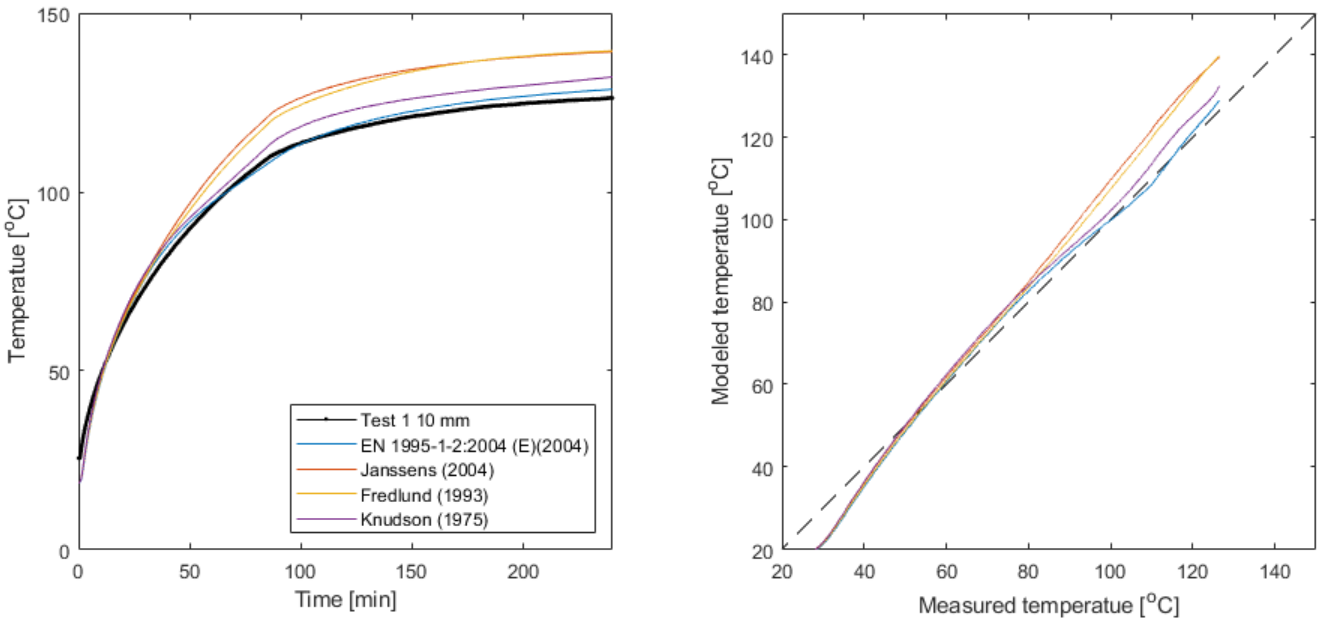

Figure 18 Comparison of the temperatures at 10 mm under the surface of the beam measured during Test 1 and those predicted by the model using different thermal properties

Figure 17 tells similar story as the temperature at previous depth but with the differences between the used thermal parameters even more pronounced. It can be concluded that thermal properties of the outer fibbers of the cross section, which can be seen from the results at 6 and 10 mm, are predicted really well with the thermal model using thermal properties provided in EN 1995-1-2:2004 (E) (2004). Significance of the heating behaviour of the outer fibbers will be discussed later in Chapter 3.2.

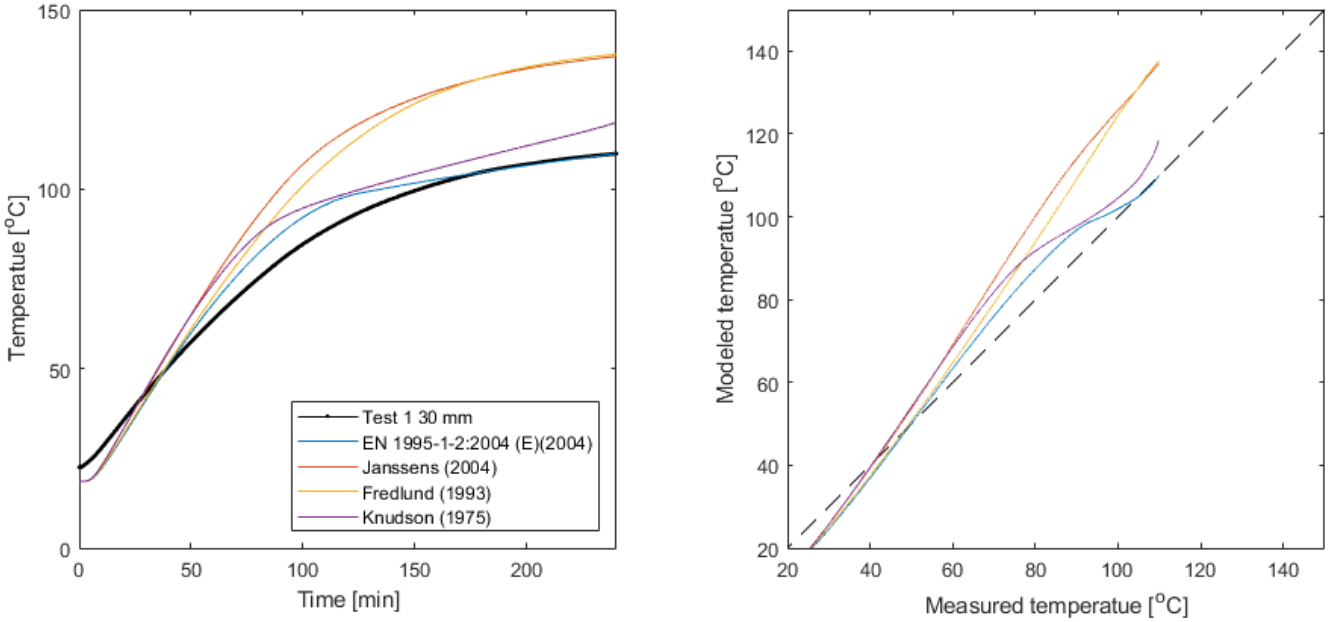

Figure 17 Comparison of the temperatures at 30 mm under the surface of the beam measured during Test 1 and those predicted by the model using different thermal properties

Figure 18 shows that at depth of the 30 mm thermal model and experimental measurements differ even more. Janssens (2004) and Fredlund (1993) based models overpredict temperatures by approximately 20%, Fredlund (1993) based one is closer with its prediction but overall trend with longer heating time is not matching the measured one. EN 1995-1-2:2004 (E) (2004) again proves as the best in matching the measured values. It has deviations of approximately 10% in the temperature range from 50 to 100°C but with the longer heating time converges to the measured values.

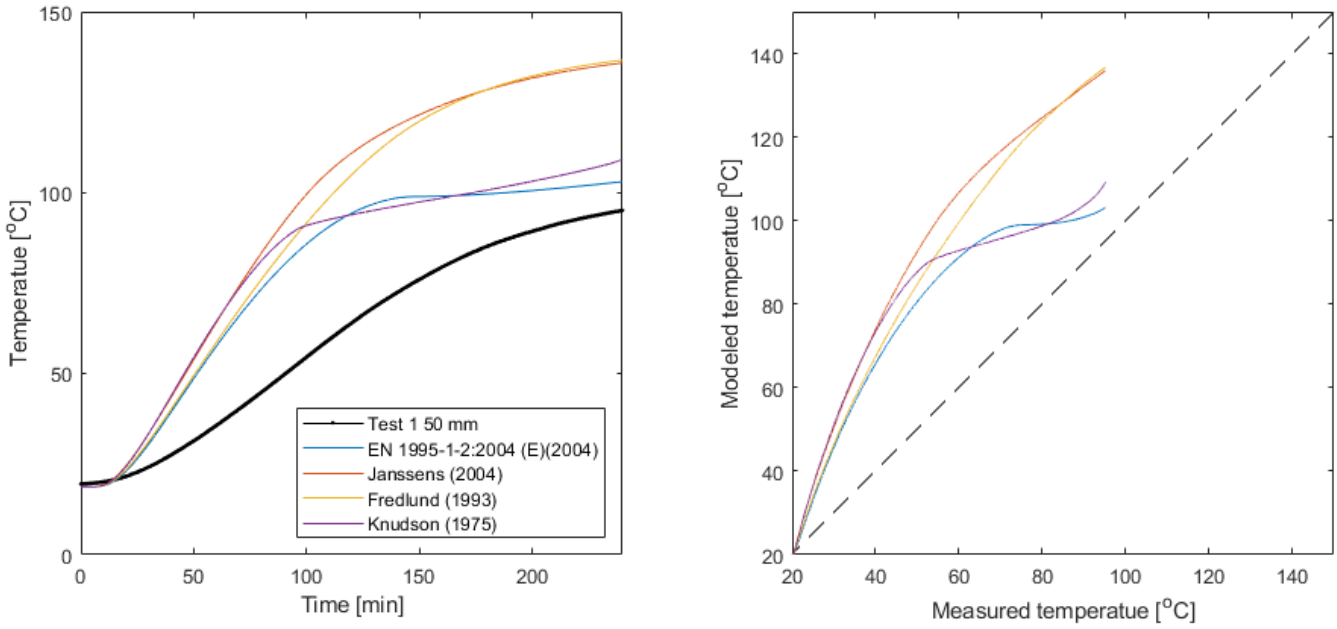

Figure 19 Comparison of the temperatures at 50 mm under the surface of the beam measured during Test 1 and those predicted by the model using different thermal properties

Figure 19 shows the biggest deviation of the thermal model from measured temperatures. Janssens (2004) and Fredlund (1993) based ones are significantly overpredicting the temperature progression. Fredlund (1993) and EN 1995-1-2:2004 (E) (2004) ones show similar behaviour and closer but still greatly overestimated temperatures compared to the measured values.

Janssens (2004) and Fredlund (1993) purposed values as mentioned earlier do not take into account energy needed for the evaporation of water. This can explain the overestimation of the temperature values predicted using them. It also explains why when using these thermal properties modelled temperatures across the cross section converge much faster than what is recorded in the experiments.

Fredlund (1993) and EN 1995-1-2:2004 (E) (2004) take into account the energy of vaporisation of water in the peak in specific heat values around 100°C shown in Figure 9. This is far better approximation of the thermal behaviour of the CLT cross section.

Bigger deviations at deeper levels of the cross section can probably attributed to the combination of two reasons. Firstly, the heating boundary conditions were assumed to be uniform across the whole beam, this might not be the case in reality. Gas temperatures at the top and the bottom of the beam could have been slightly different causing non-symmetrical thermal gradient trough the cross section. This was not recorded as the thermocouples were positioned at the top half of the beam only.

Second possible cause of the bigger deviations at bigger depth could be moisture transfer inside of the beam. It was already mentioned that the thermal model does not take into account mass transfer trough the material. In reality due the heating of the material moisture evaporates and in the form of steam moves deeper trough the centre of the beam where the temperatures are lower and cause it to condensate. This phenomenon could possibly explain slower heating of the central parts of the beam than those predicted by the thermal model.

The same comparison was made for all four tests with similar results and they are presented in Appendix. For Test 4, in which the specimen used had the same cross layer configuration as the one used in Test 1, the thermal model predictions and measured differences almost the same as one ones presented above for Test 1. For Test 2 and 3, which had three-layer configuration, results are not as consistent as for the previously mentioned ones. Behaviour was similar for all depths except the 30 mm one. This can possibly be attributed to either non-ideal thermocouple positioning or two times bigger layer thickness compared to the five-layer configuration. For timber, with the thickness of the layer possibility of knots, faults or any other material inconsistencies rises.

Temperatures measured at the depths of 10 mm but at different positions along the beam's main axis (Figure 14) showed temperature difference of order of magnitude 1-2°C for all four tests, demonstrating that the previously stated assumption of constant temperature gradient along the beam's longitudinal axis is appropriate.

Temperature data obtained from the thermocouples positioned off the beam's main axis show many inconsistences between four tests and also compared to the thermal models predictions. The cause of these inconsistences was not determined and it was ignored during the analysis as its influence on the later analysis is not significant, but it is noted here and the data is presented in Appendix.

3.2 Stiffness model

After the analysis of multiple thermal properties for the thermal model, values from EN 1995-1-2:2004 (E) (2004) were implemented for all further analysis. As it was presented earlier in Chapter 1.3, in the literature numerous function of reduction of modulus of elasticity of timber with elevated temperature were presented. Based on those data nine different reduction functions were implemented in the stiffness model. All models are presented in Figure 20. In the case of König (2000) and Thomas (1996) different functions for compression and tension modulus were used and presented, the dashed line presents the mean value. When the authors did not provide the values for temperatures as high as 300°C it was assumed that reduction remains constant after the last known point. This analysis due to the limitations of the heating chamber used in tests only the temperatures up to 140°C for which all the regarded authors provided values.

Figure 21 show reduction of the bending stiffness of the cross section for the beam used in Test 4 predicted by the stiffness model using different modulus of elasticity reduction functions. The input for the model was the temperature gradient obtained from the thermal model for the gas temperature recorded during the experimental test. It shows a wide distribution of results but it can be noted that excluding reductions provided by König (2000), Thomas (1996) and Glos & Henrici (1991), all other purposed modulus of elasticity reduction functions show results in the range of approximately 8%.

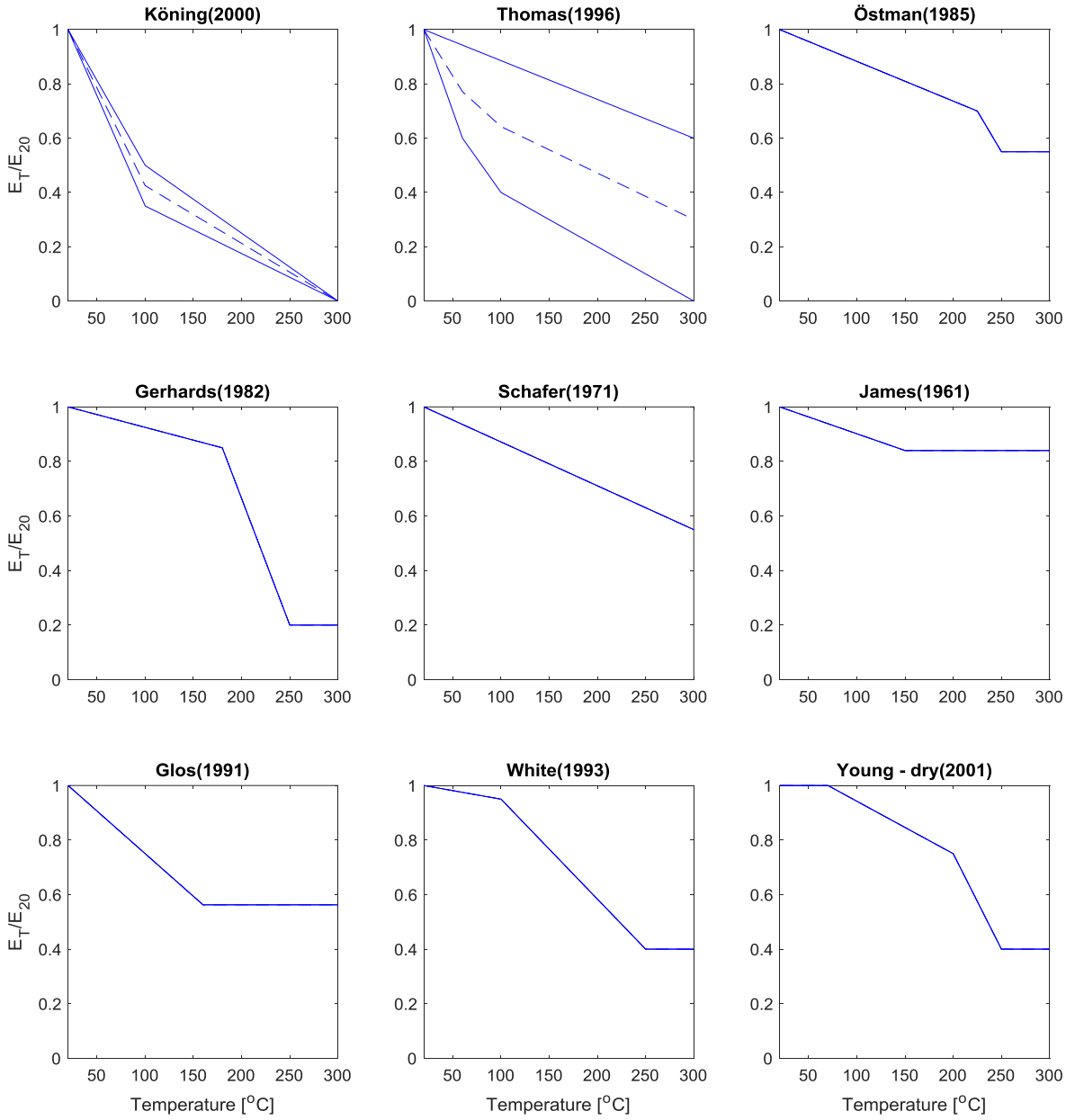

Figure 20 Reduction of modulus of elasticity – temperature functions used for the stiffness model

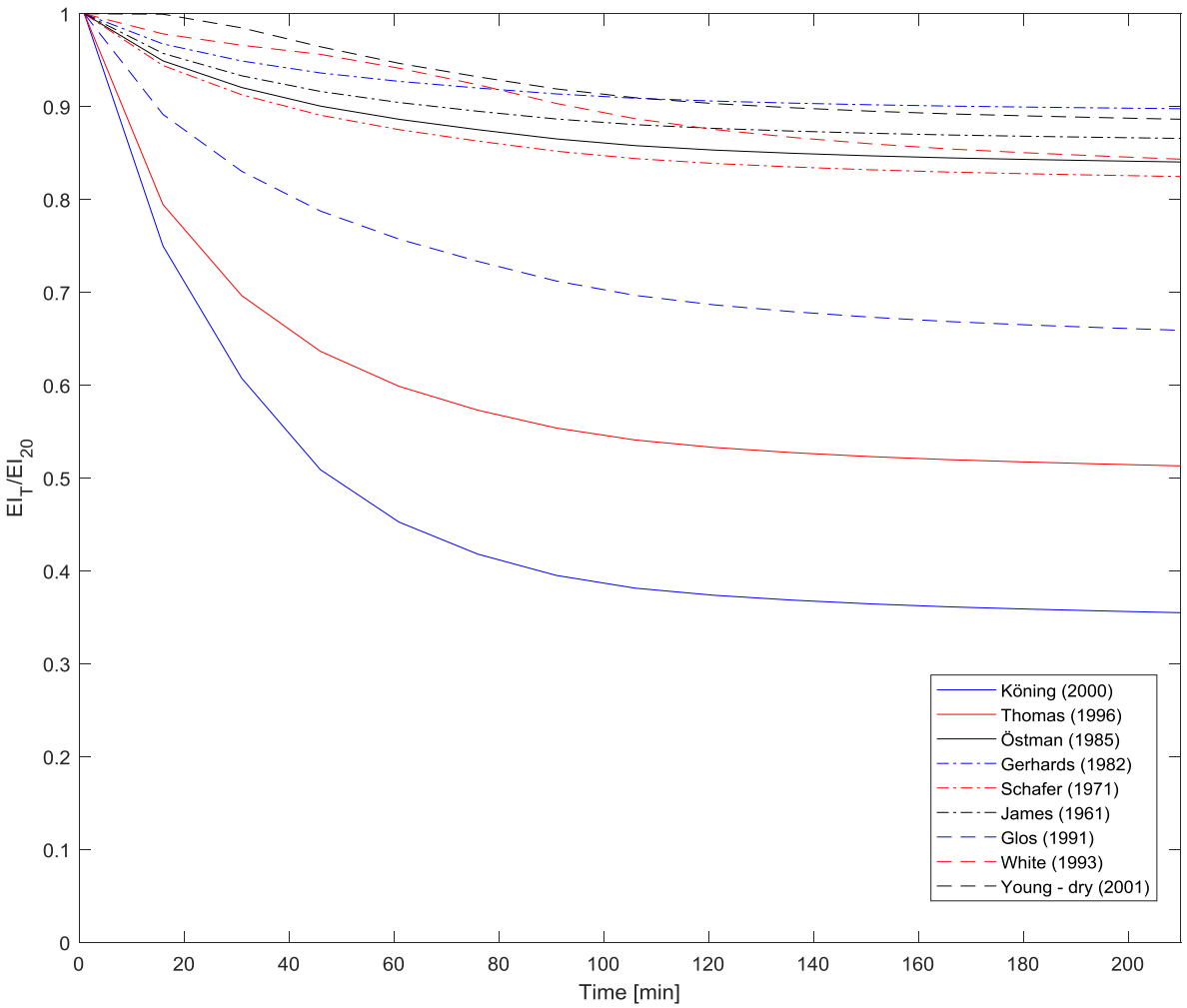

Figure 21 Reduction of the bending stiffness for the beam used in Test 4 predicted by the stiffness model using different modulus of elasticity reduction functions found in literature.

Before doing the experimental tests, in order to get an idea how the beam will behave and what are the best positions inside the cross section for the thermocouples for assessing the reduction of the modulus of elasticity, following analyses has been undertaken. Temperature gradient inside of the cross section is not uniform and that makes acquiring direct function of the reduction of modulus of elasticity with temperature difficult. In order to achieve this the task of determining an equivalent temperature for the whole cross section was undertaken. This temperature would present the temperature that should be uniform over the whole cross section in order for the same stiffness reduction to be achieved as for a given thermal gradient.

This was done by taking the calculated stiffness reduction and using the reduction function used for its calculation to calculate for which temperature that same reduction of modulus of

elasticity is achieved. After this equivalent temperature was calculated, the thermal gradient over the cross section was analysed in order to find spot on the cross section with that same temperature. It was determined that spot was positioned at vertical axis of symmetry of the cross section at approximately 6 mm beneath the surface for all different modulus of elasticity reduction functions.

To show the significance of this equivalent temperature on the Figure 22 reduction of the stiffness of the cross section was plotted versus the temperature at 6 mm from the surface of the beam. Alongside it, the used functions of reduction of modulus of elasticity were also plotted. It can be observed that according to the stiffness model the temperature at this position can be used to relatively accurately present the reduction the modulus of elasticity. This analysis Is based purely on the thermal and stiffness models and only uses gas temperature from the tests as an input in the thermal model.

Position of the equivalence temperature spot on the cross section can be explained to some extent with the nature of the bending stiffness of the CLT cross section. Figure 23 and Figure 24 show how much each part of the cross section influences bending stiffness of the whole cross section. It can be seen that outer parts have biggest influence, when that fact is coupled with the fact the temperatures there are also highest, a conclusion can be drawn that the position of the equivalence temperature spot is going to be in the 10% of the cross section furthest from the centre.

Furthermore, it can be concluded that bad prediction of the central temperatures of the thermal model, mentioned in Chapter 3.1 does not have significant influence on predicting the reduction of stiffness with elevated temperatures.

Based on all of this, for the experimental tests the thermocouples were positioned at the 6, 10, 30 and 50 mm from the surface in order to capture the temperature gradient in the cross section and also provide suitable information for assessing the reduction of the modulus of elasticity with elevated temperature.

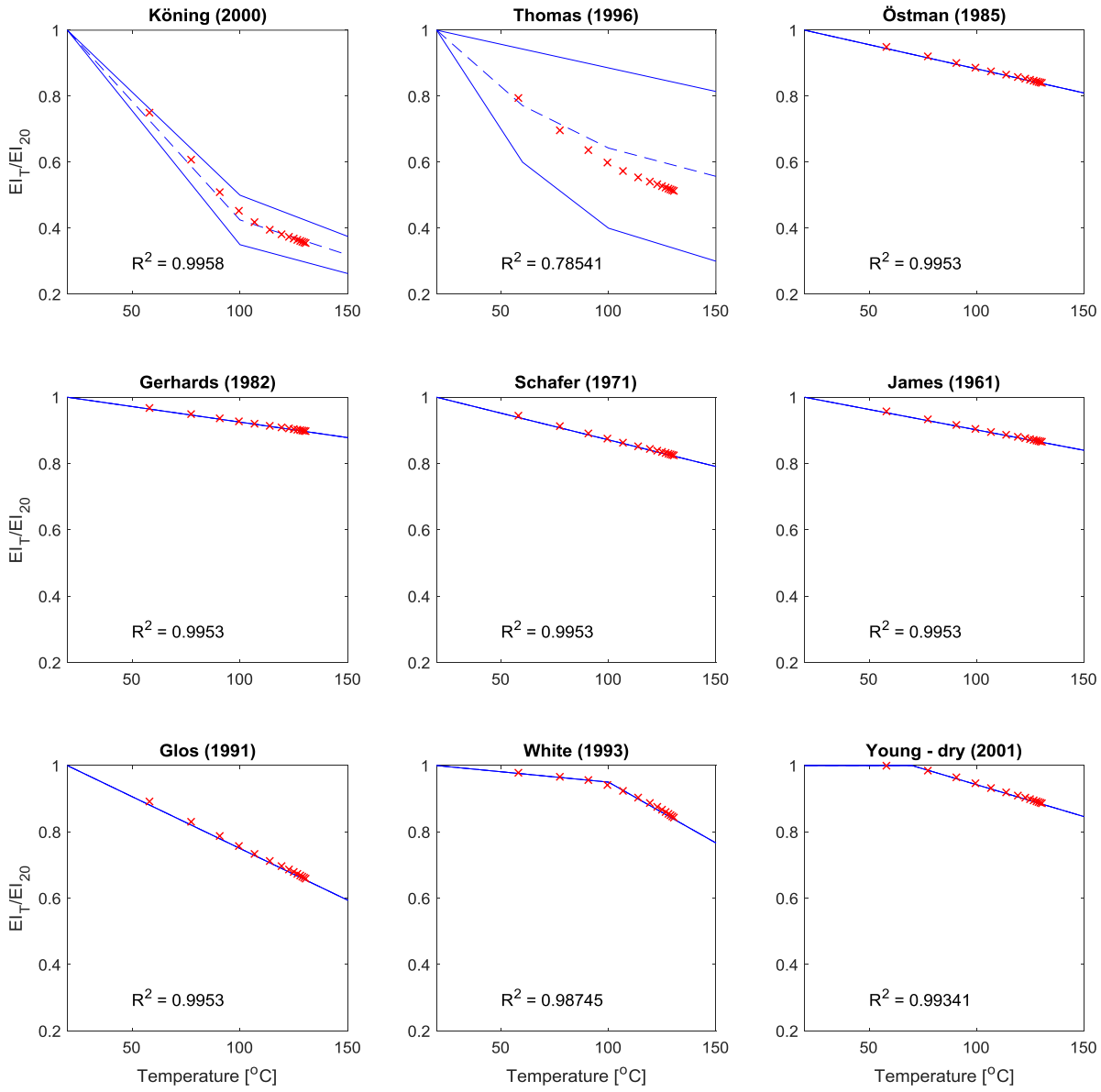

Figure 22 Reduction of the stiffness of the cross section was plotted versus the temperature at 6 mm for the surface (red) plotted alongside the modulus of elasticity reduction functions used (blue)

Figure 23 Influence of each layer to the total bending stiffness for the five layer configuration

Figure 24 Influence of each layer to the total bending stiffness for the three- layer configuration

Figure 25 and Figure 26 are graphically presenting the influence of the elevated temperature on the bending stiffness of the cross section. These figures were made by reducing the width of each horizontal 1 mm layer of the cross section by how much each modulus of elasticity of each cell located in that layer has been reduced. (Also the perpendicular layers have their width reduced by additional factor of 30 due to the assumption that modulus of elasticity in perpendicular direction is 30 lower than in the direction parallel to the grain). This way the shape of the “effective” cross section is presented.

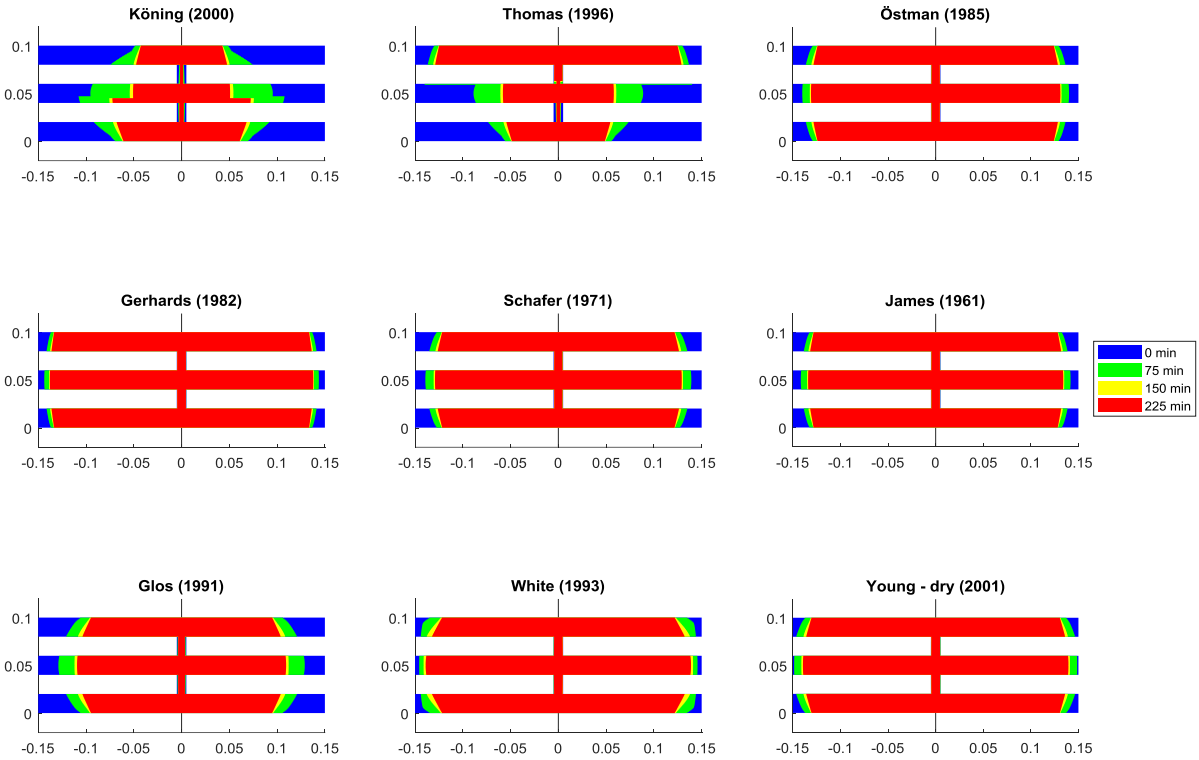

Figure 25 Effective cross section progression over time for different modulus of elasticity reduction functions for the five-layer cross section

Alike to what was concluded from the Figure 21, it is obvious that the cross section behaves similarly for all purposed reduction functions except for those by König (2000), Thomas (1996) and Glos & Henrici (1991). Unsymmetrical for the König (2000), Thomas (1996) cases is consequence of the different reduction for compression and tension. This, as the case of the pure bending is considered, moves the neutral axis away from the centre and creates an asymmetric effective cross section.

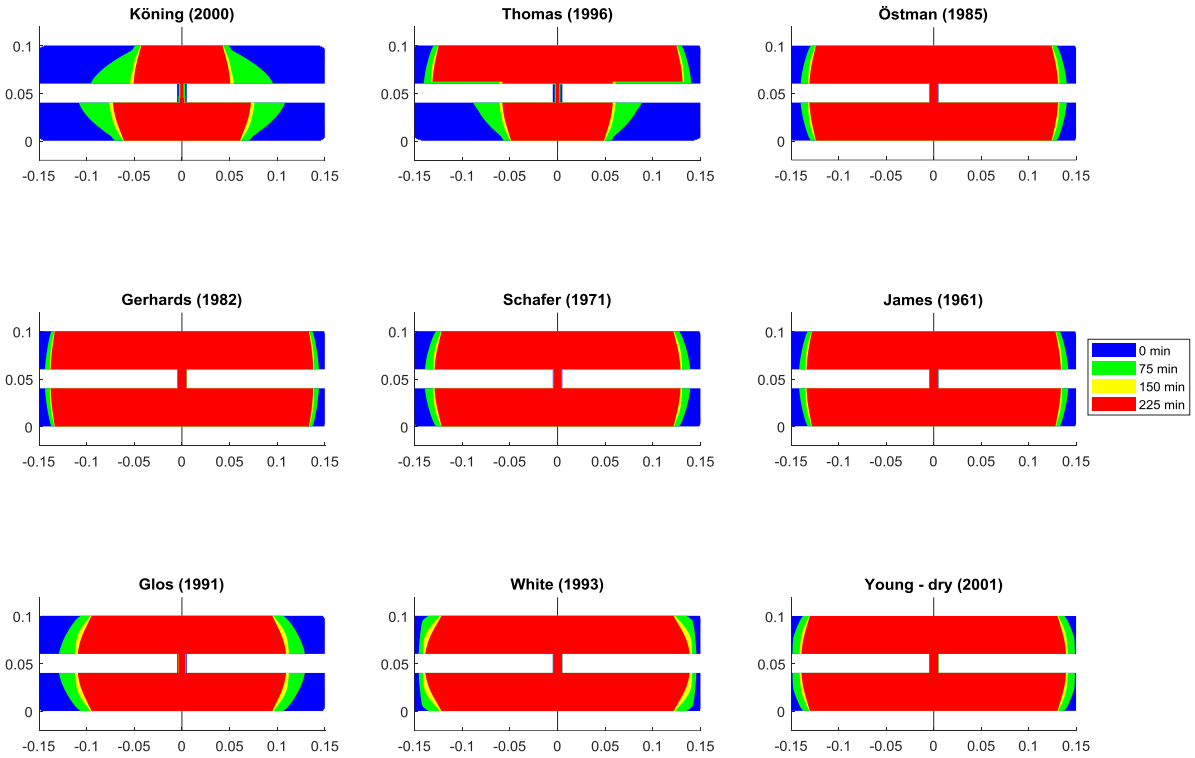

Figure 26 Effective cross section progression over time for different modulus of elasticity reduction functions for the three-layer cross section

3.3 Experimental results

As it was previously mentioned in the Chapter 2.3, reduction of stiffness was measured using modal analysis. In order to do it acceleration time history was recorded after the beam was excited by an impulse force. Because of the sensitivity of the high temperature accelerometer attached to the beam alongside the oscillation of the beam as the response from the impact, response of due to the fan used for the heating of the chamber was recorded. Fortunately, the frequency of the fan was several times larger than the natural frequency of the beam. A low pass digital filter was used to filter out the effects of the fan and provide better representation of the response of the beam. On the Figure 27 an example of the filtering is presented. The cut off frequency used was 60 Hz as the first natural frequencies of the tested beams were expected to be in the range of the 30±5 Hz.

For the analysis of the signal and in order to obtain the dominating frequency Matrix pencil method for estimating parameters of exponentially damped sinusoid in noise was used. It is a special case of the matrix prediction approach and has been shown to be more efficient in computation, less restrictive about signal poles, and less sensitive to noise for signals with unknown damping factors than the polynomial method (Hua & Sarkar (1990)). The MATLAB (2016) script used for his analysis was taken from Zieliński & Duda (2011). It is based on the time domain and in essence fits prescribed number of damped sinusoids on the measured signal to get its best approximation. Figure 28 shows an example of this curve fitting and show a distinctive dominant frequency in the magnitude and phase graphs.

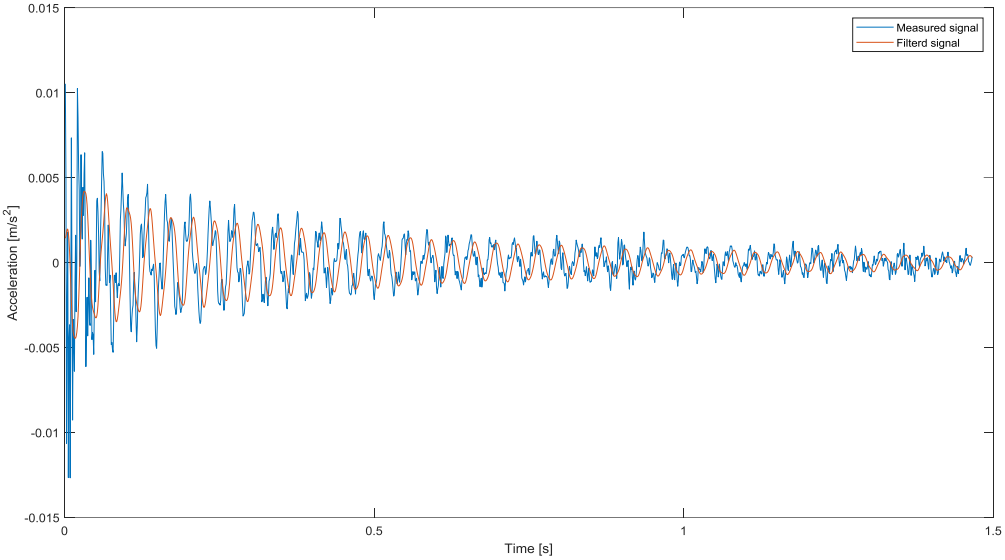

Figure 27 Example of the measured signal before and after filtering

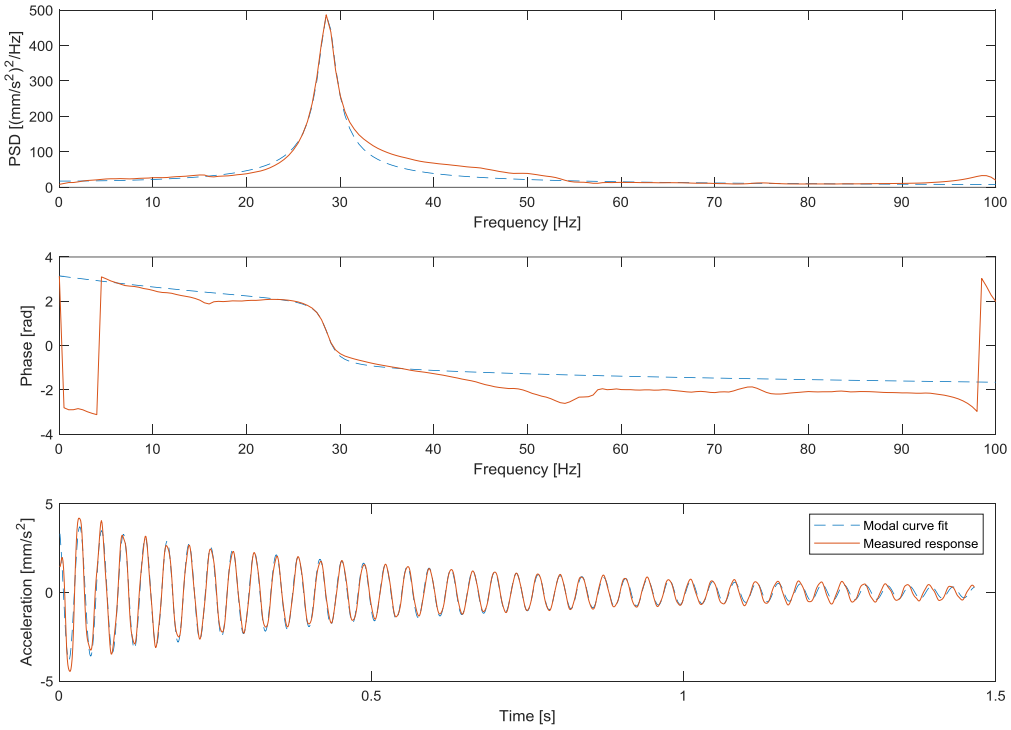

Figure 28 Example of the determination of the dominant frequency of the accelerometer signal

Each test lasted at least four hours and the moments where the sample beam is excited have been chosen arbitrary. At the beginning of the heating, they were chosen approximately when the temperature 6 mm form the surface rises for 10°C, up until the temperature of 90°C, when the interval was lowered to 5°C. The temperature at 6 mm from the surface starts to

raises much slower after it achieves 120°C so after that the excitation moments were chosen to be approximately every 15-20 min. That explains why there is a much larger concentration of data points in the beginning of the test.

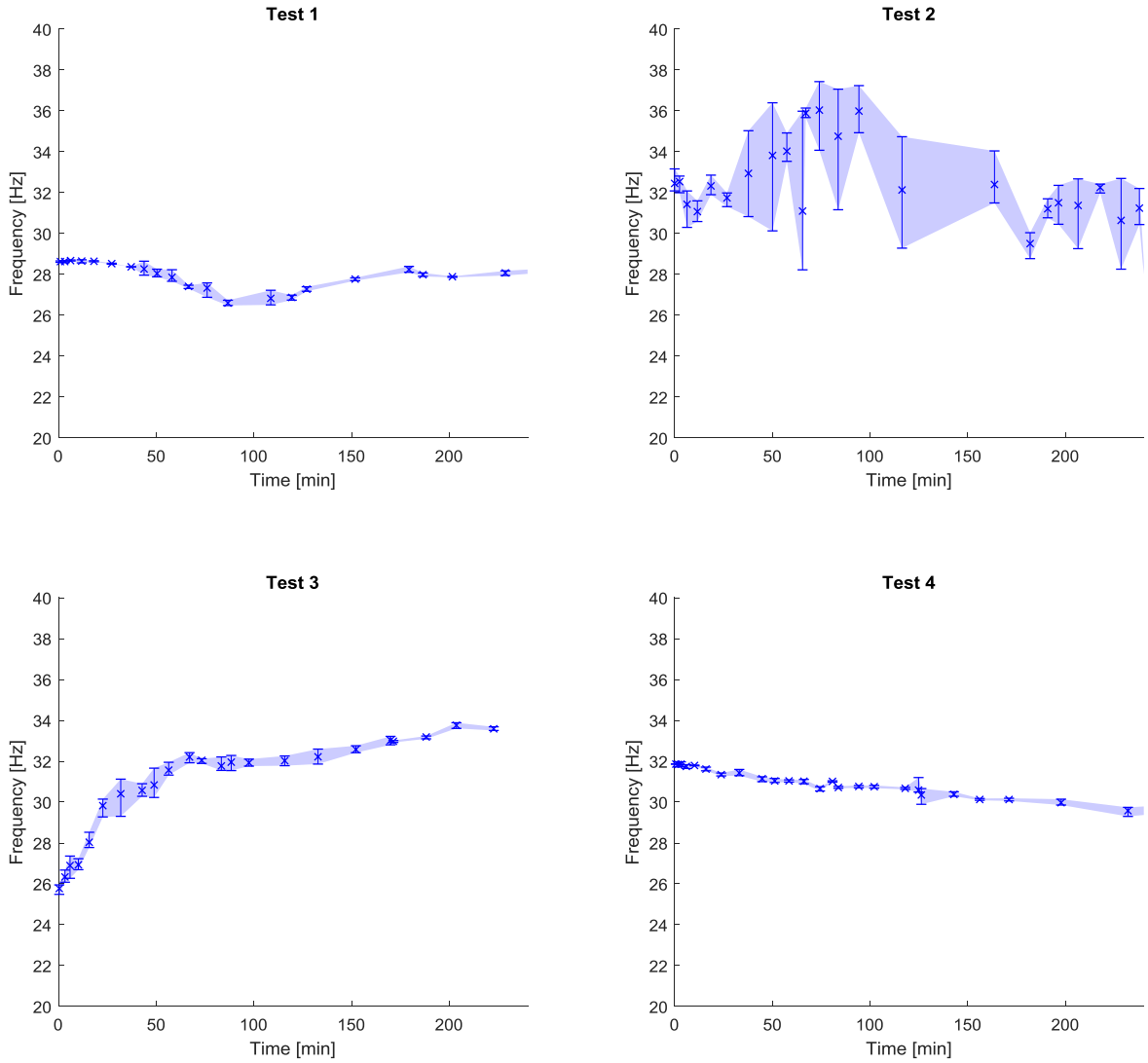

Figure 29 Measured natural frequencies for all three tests - Error bars and shaded area represent the variation of the measured frequencies at that moment

As it was mentioned in the Chapter 2.3 every time the accelerometer response was measured, the beam was excited with a hit at least three times. That way the frequency at that moment in time was determined as the average of those three or more frequencies. At the Figure 29 that variation of the measured frequencies was presented with error bars and shaded area. It can be noted that the variation in the Test 1 and 4 (in both cases the five-layer

beam was used) is relatively small and that the measured and do not excide ±2% and was less than ±0.5% for most points. For the Test 3 variation is more pronounced but it does not excide ±4%. For the Test 2 it is evident that measured results vary much more, for some data points up to ±15% . In addition, contrast to other tests in Test 2 no obvious trend is present which is probably the consequence of such a variance of the measured frequencies at each point in time. It should also be noted that as presented in Chapter 1.3, it is expected that the stiffness, and therefore natural frequency, reduces only for few percentage for duration of the whole test and thus precision of the frequency measurements is needed.

Possible reason for the great variability of the results for Test 2 is noted sleight torsional deformation of the beam used. It was observed that when the beam was positioned on the supports in the heating chamber it did not completely stable. When the beam was hit, a sleigh torsional rotation was observed. That rotation could induce error into frequency measurements as it would interfere the acceleration recorded by adding significant rotational component. Results of the Test 2 are still going to be included in the further analysis, but will mostly regarded as unreliable.

To determine how much the stiffness of the cross section has been reduced Equation (15) is used. As the ratio of the stiffness at elevated temperature and at ambient temperature (20 °C) is of the biggest importance it can be derived from following form:

$$\frac{EI_T}{EI_{20}} = \left(\frac{f_T}{f_{20}}\right)^2 \cdot \frac{m'_T}{m'_{20}} \qquad (22)$$

It is evident that to obtain the reduction of stiffness the ratio of mass change has to known. The heating chamber used for experiments did not allow for the monitoring the mass during the test. To overcome this obstacle data from the thermal model was used. To elaborate, thermal model used the function of how much the density of wood reduces with elevated temperatures. This is the consequence of moisture evaporating and escaping the beam. Output from the thermal modes among others, produces how the mass of the cross section changes over time, by summing the temperature dependent density across the cross section. This data was used to obtain the information on how much has the mass reduced during the test.

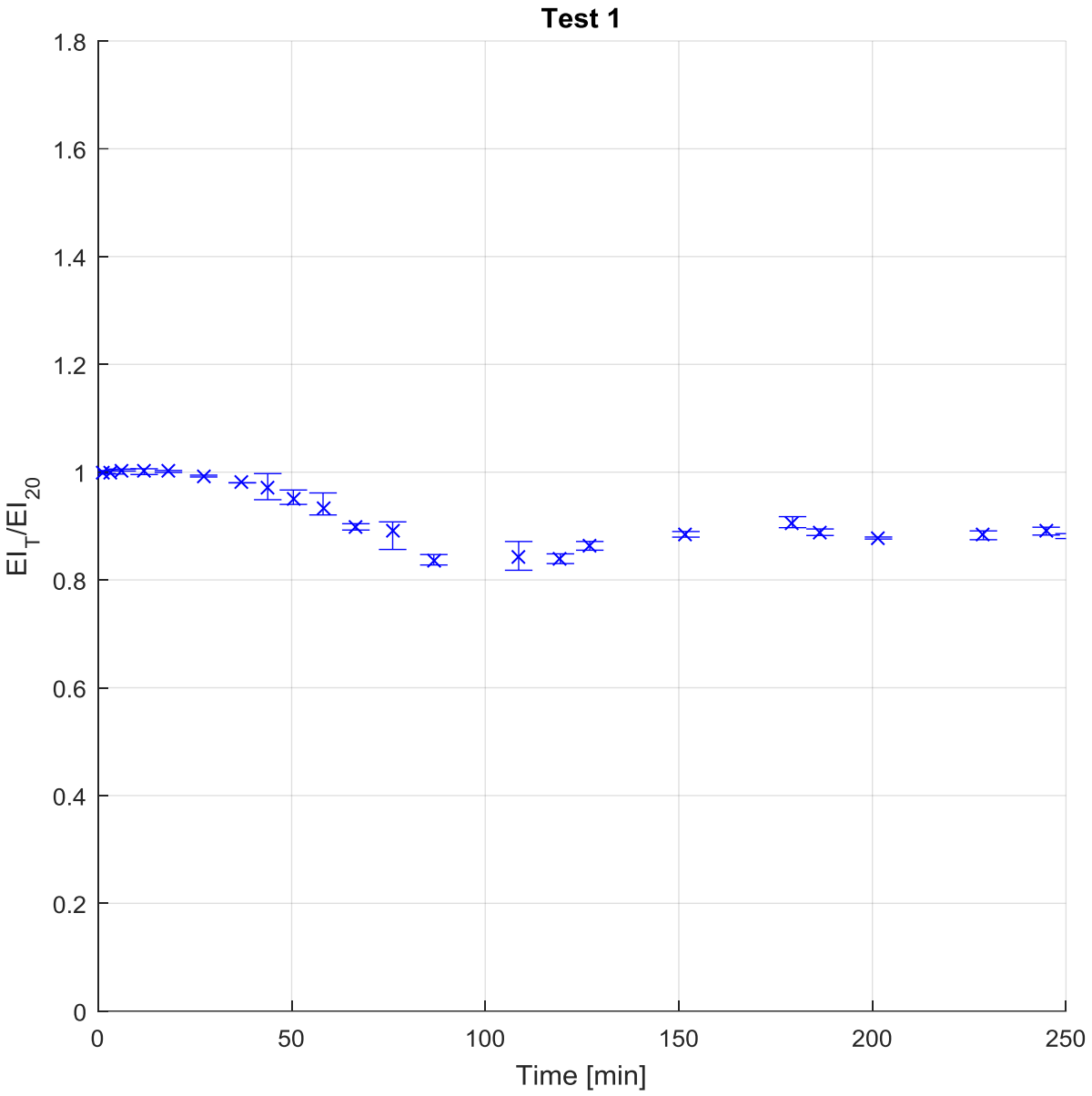

Figure 30 Reduction of bending stiffness trough time for the Test 1 (five-layered configuration)

Figure 30 shows measured bending stiffness reduction for Test 1. Two regions are clear, first, in the first 100 min the stiffness reduces almost parabolic up to the value of 84% of the value at ambient conditions. Afterwards the stiffness starts to increase almost linearly to the value of 89% of the original value. It should be noted that moment in time when the behaviour of the stiffness of the beam changes, relatively corresponds with the moment when the temperatures of the whole outer layer, with the grains parallel to the main beam's axis, excide 100°C. There was no thermocouple on the edge of the outer layer (20 mm), but this was determined based on the interpolation of the temperature data from measured depths.

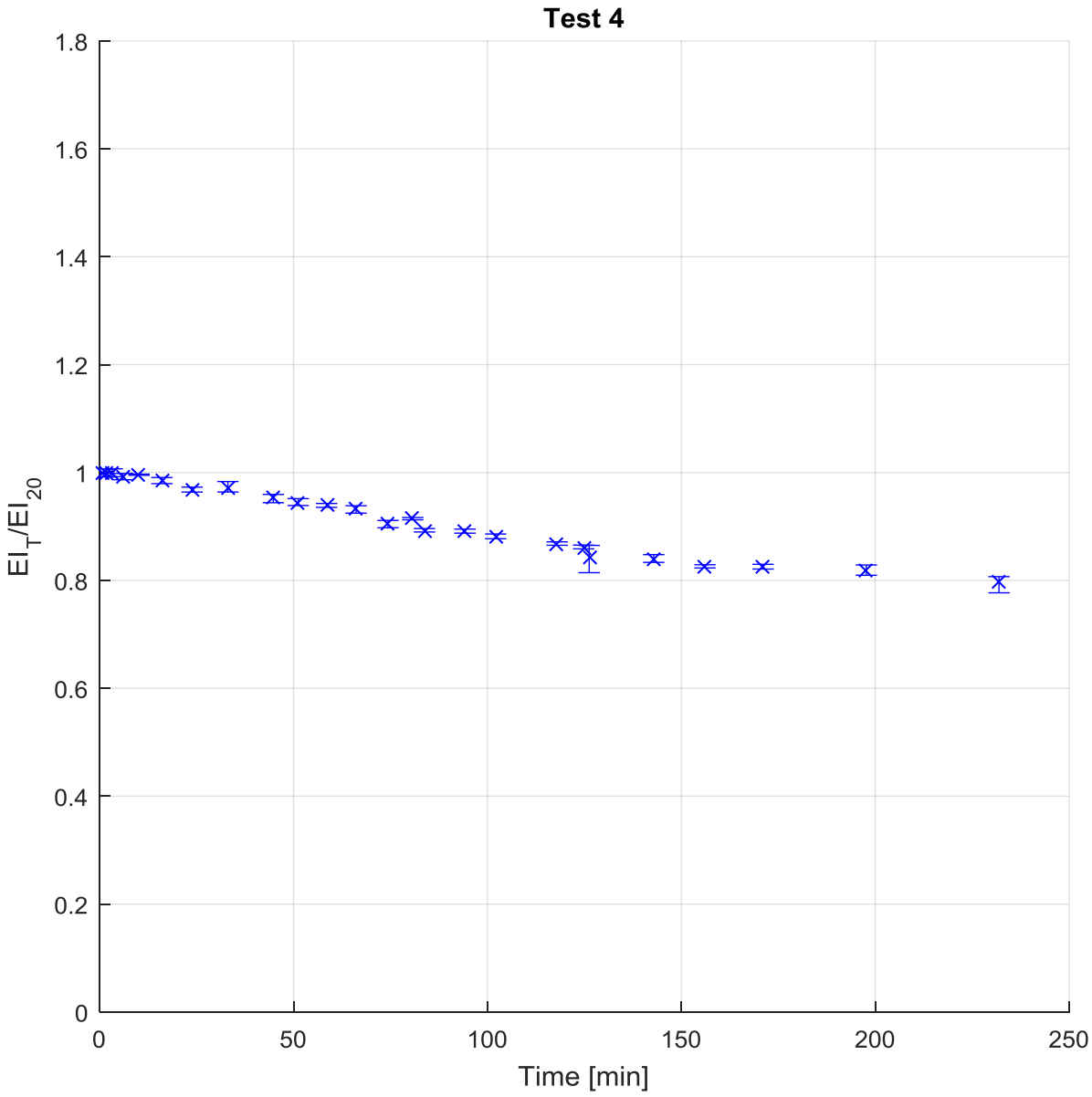

Figure 31 Reduction of bending stiffness trough time for the Test 4 (five-layered configuration)

Figure 31 shows stiffness reduction for the Test 4, also a five-layered configuration. It can be observed that similar results are obtained in the first 100 min as for the Test 1, reduction follows a more linear trend and drops to approximately 88% at same time. In contrast to the Test 1, stiffness of the beam continues to reduce linearly until it drops to almost 80% around 230 minute mark.

It should be noted that at ambient temperature measured bending stiffness of the beam used in Test 4 was almost 25% bigger than the one measured for the beam used in Test 1. Even though both beams came from the same source and had same layer configuration, this

difference can be attributed to the wide variability of mechanical properties of timber as a material.

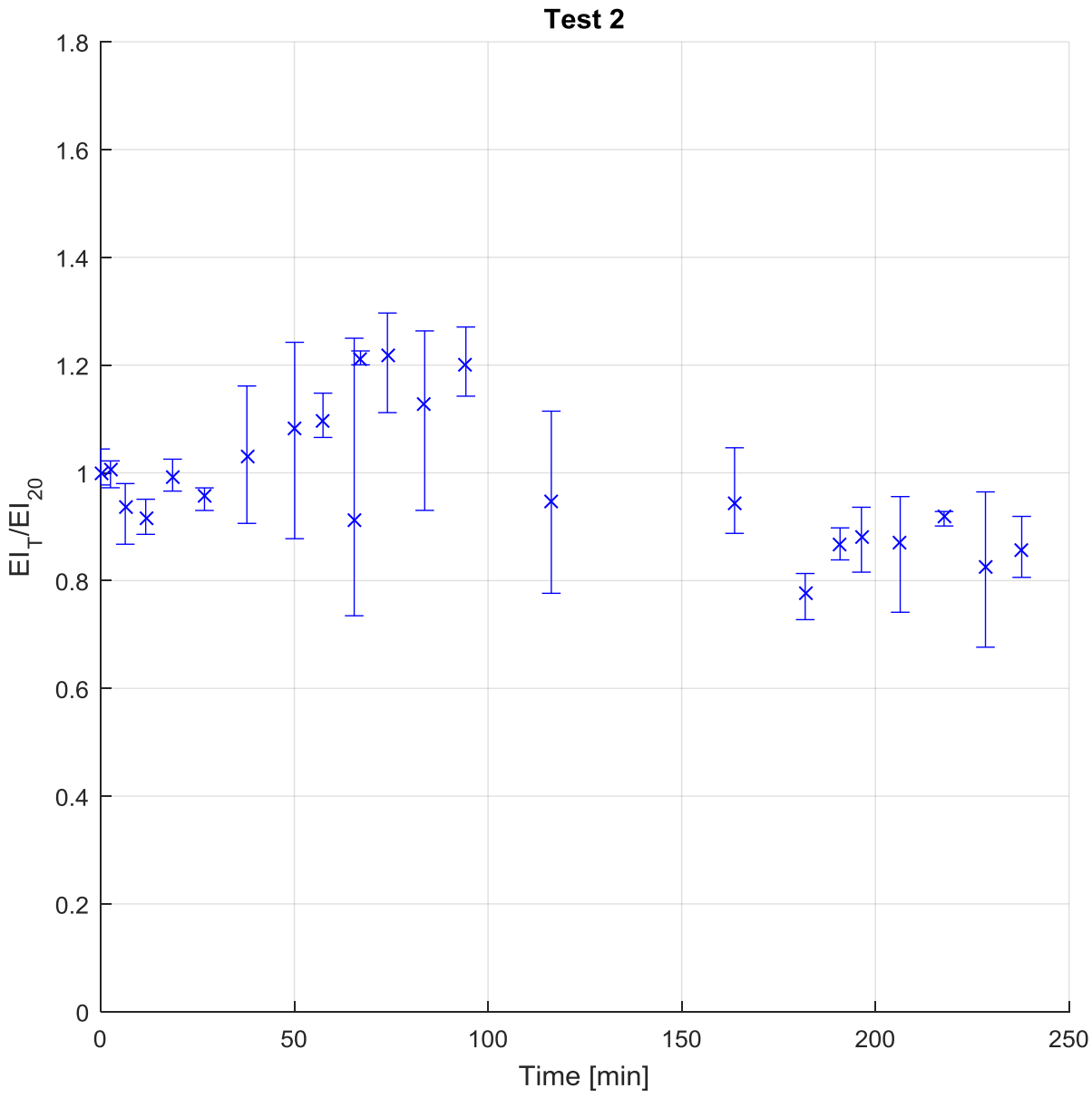

Figure 32 Reduction of bending stiffness trough time for the Test 2 (three-layered configuration)

Figure 32 shows reduction of bending stiffness trough time for the Test 2 (three-layered configuration). As it was already stated earlier measurements vary substantially and no clear trend can be observed. With that being said, some vague trend can be noted, as the values at the second part of the test show lower values, but reliability of these results is highly questionable.

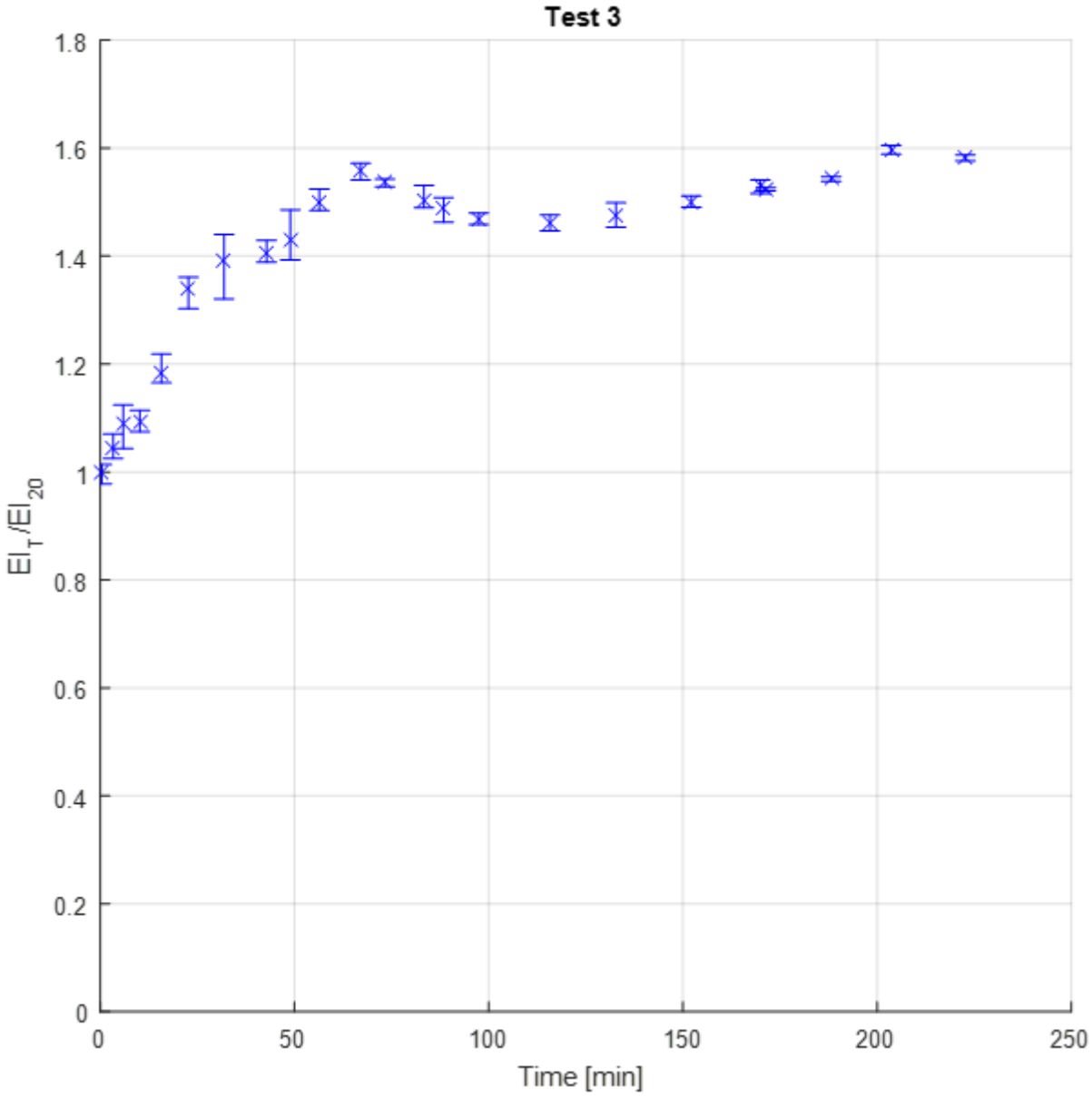

Figure 33 Reduction of bending stiffness trough time for the Test 3 (three-layered configuration)

Figure 33 shows stiffness reduction for the Test 3, a three-layered configuration beam. As it is clearly evident test sample behaved significantly differently than the ones in Test 1 and 4. Instead of the reducing, like it was the case for Test 1 and 4, the bending stiffness in this case increases with time. Those stiffness variations are considerably bigger than in previous cases, with the peak value being almost 60% bigger than the one recorded in the ambient conditions. In addition a clear linear increasing trend is evident until approximately 60 min from the start of the test after which the value decreases until the 100 min mark. At that point it shows similar behavior as the one recorded for the Test 1 at that point.

During the test nothing out of the ordinary was observed that could explain the drastically different recorded behavior from that recorded in other tests or from what was usually found in the literature.

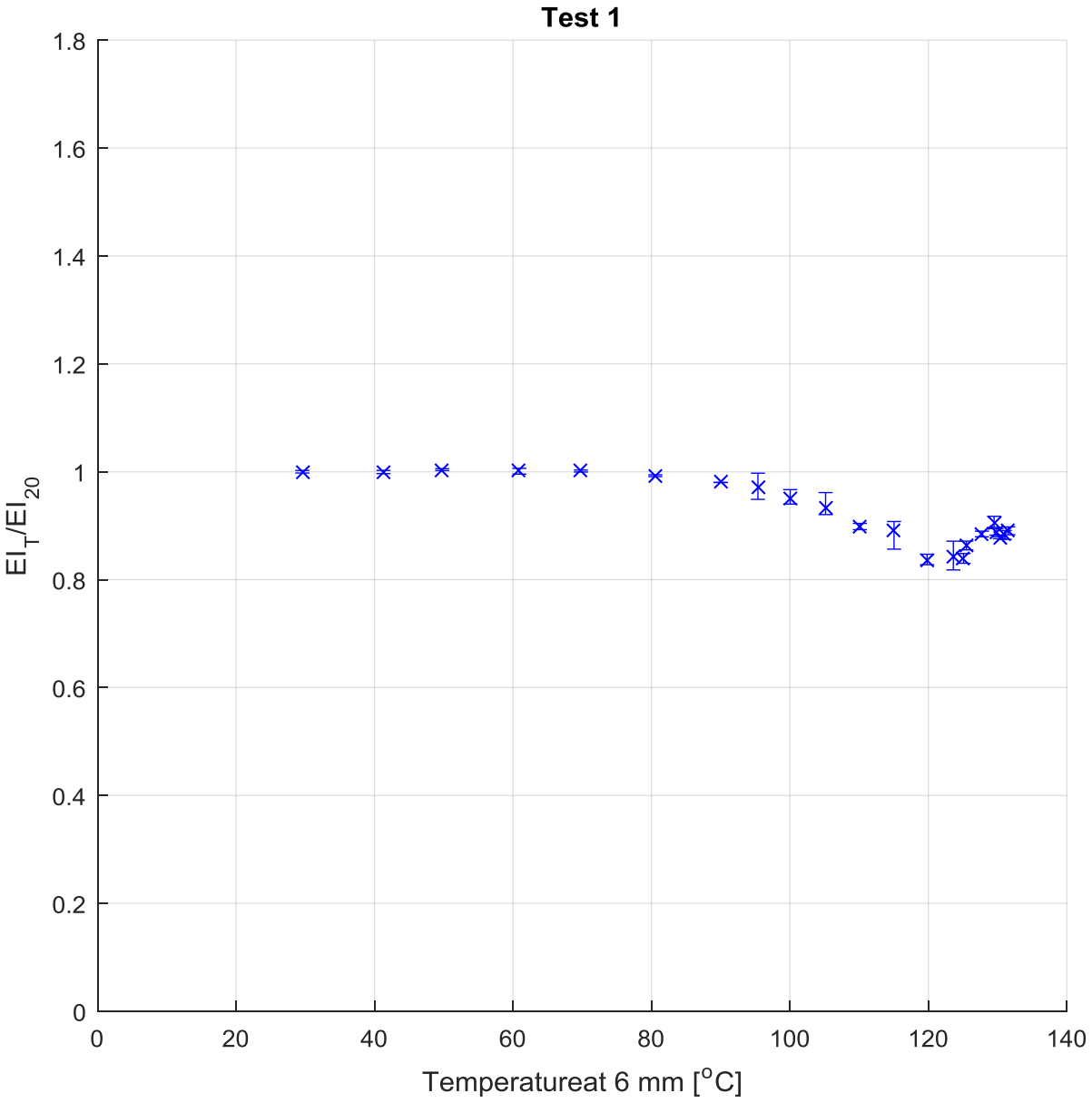

Figure 34 Reduction of bending stiffness plotted against temperature at 6 mm from the edge of the cross section for the Test 1 (five-layered configuration)

Using the previously explained method of presenting the reduction of modulus of elasticity with elevated temperature derived from the model's results. Figure 34 shows this way of representing results for the Test 1. Three regions are evident: first the almost constant until 80°C, second with the drop until 120°C and at the end rise until the end of the test. On Figure 35 results for Test 4 are presented and also shows three distinctive zones. First two zones

behave almost the same as for the Test 1, with the biggest difference in the third zone, after 120°C, where the values drop.

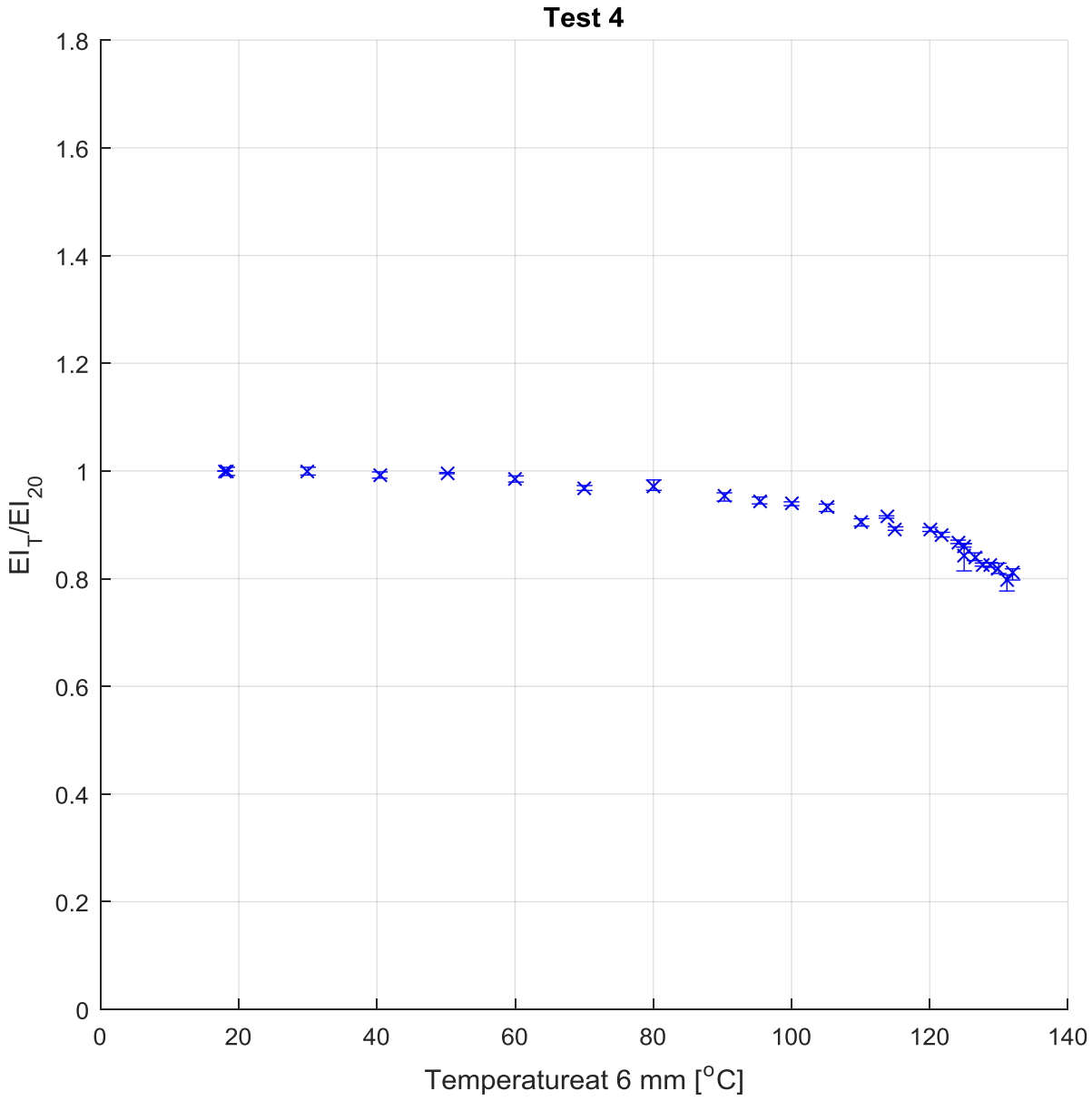

Figure 35 Reduction of bending stiffness plotted against temperature at 6 mm from the edge of the cross section for the Test 4 (five-layered configuration)

The results for Test 2 are presented on Figure 36 and are as stated above not reliable. Nevertheless, when analyzed in previously stated three zones, in the first zone variance is lower compared to the second zone, and reduction is relatively constant. In the second zone the results vary significantly more and in the last zone values drop and they vary relatively less.

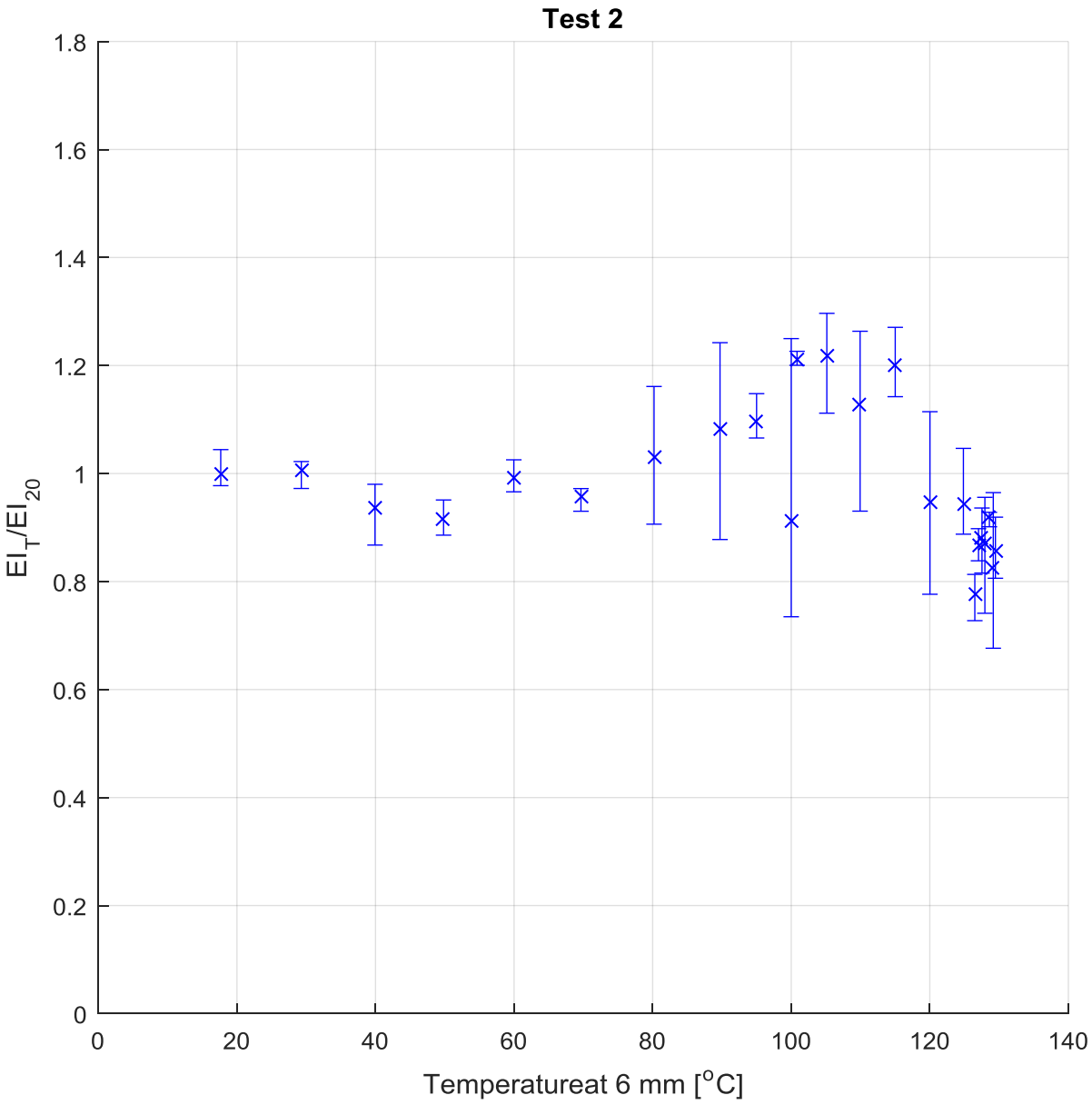

Figure 36 Reduction of bending stiffness plotted against temperature at 6 mm from the edge of the cross section for the Test 2 (three-layered configuration)

For the Test 3 results are presented on Figure 37. Again, three zones are clear but their boundaries and characteristics are different. Firstly, there is a rising zone until 105°C, flowed with the decreasing zone until 120°C and at the end rising zone until the end of the test, similarly as for the Test 1.

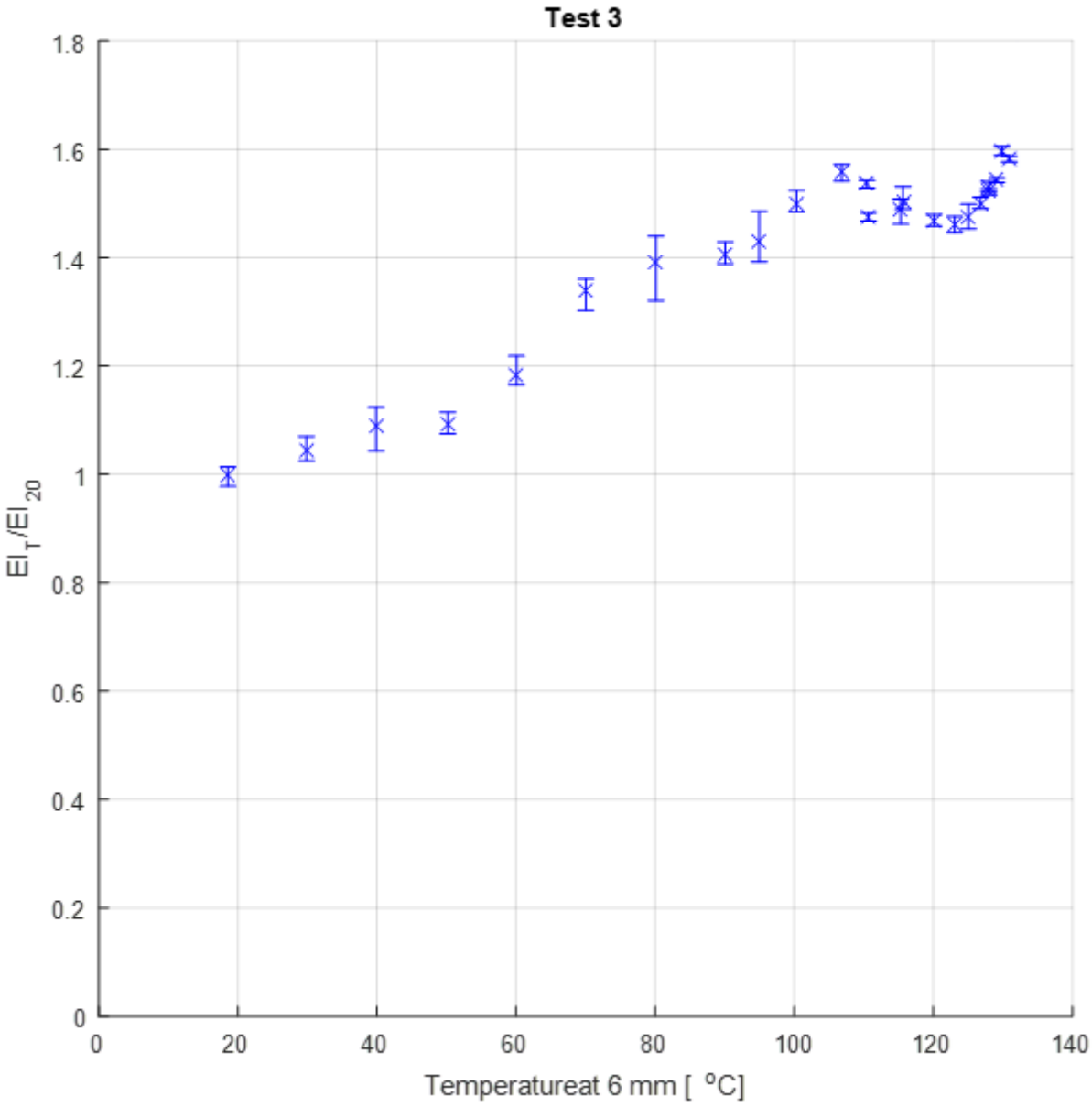

Figure 37 Reduction of bending stiffness plotted against temperature at 6 mm from the edge of the cross section for the Test 3 (three-layered configuration)

The increasing of the measured natural frequency and therefore bending stiffness recorded during the Test 3 is highly unexpected. Neither results from Tests 1 and 4 nor previously reported results of the change of the modulus of elasticity of timber with elevated temperature, state that stiffness of the beam would increase. With that in mind there is a bigger possibility that this recorded behavior is a consequence of the method used to evaluate bending stiffness with elevated temperature used in this study than the property of the material itself.

Possible insight into this problem can be measured acceleration signal presented on Figure 38. It shows how measured and filtered signals at ambient temperatures look for Tests 4 and 3. It is clear that in the Test 3 signal there is a strong presence of second frequency, which in this case is equal to approximately 100 Hz and is 4 times bigger than the frequency. This frequency has a much bigger amplitude and corresponds with the frequency of the fan as it is constant and present during the test. It also corresponds to the second natural frequency of the beam, which can cause its resonance. This does not explain the observed behavior, but can present a clue in its explanation.

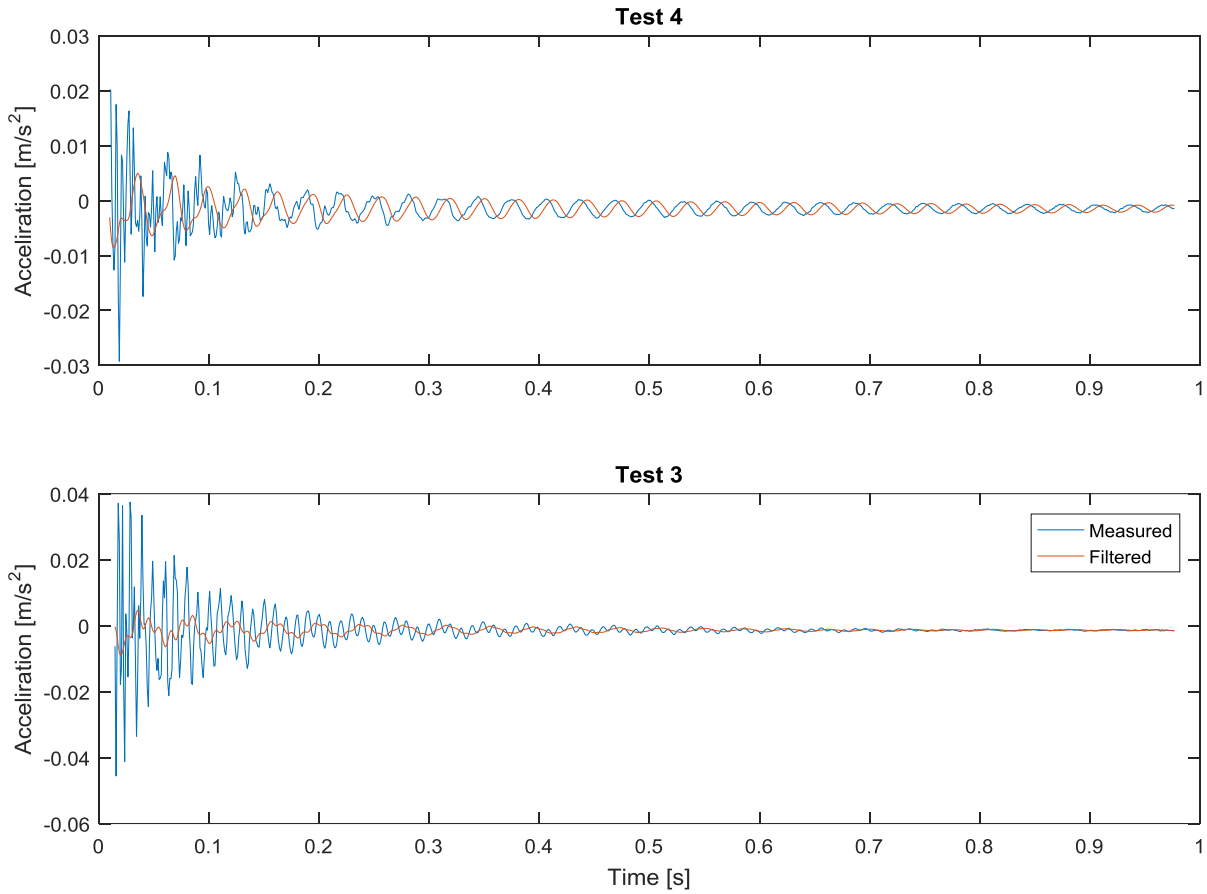

Figure 38 Comparison of the measured acceleration signal at ambient temperature from Test 4 and Test 3

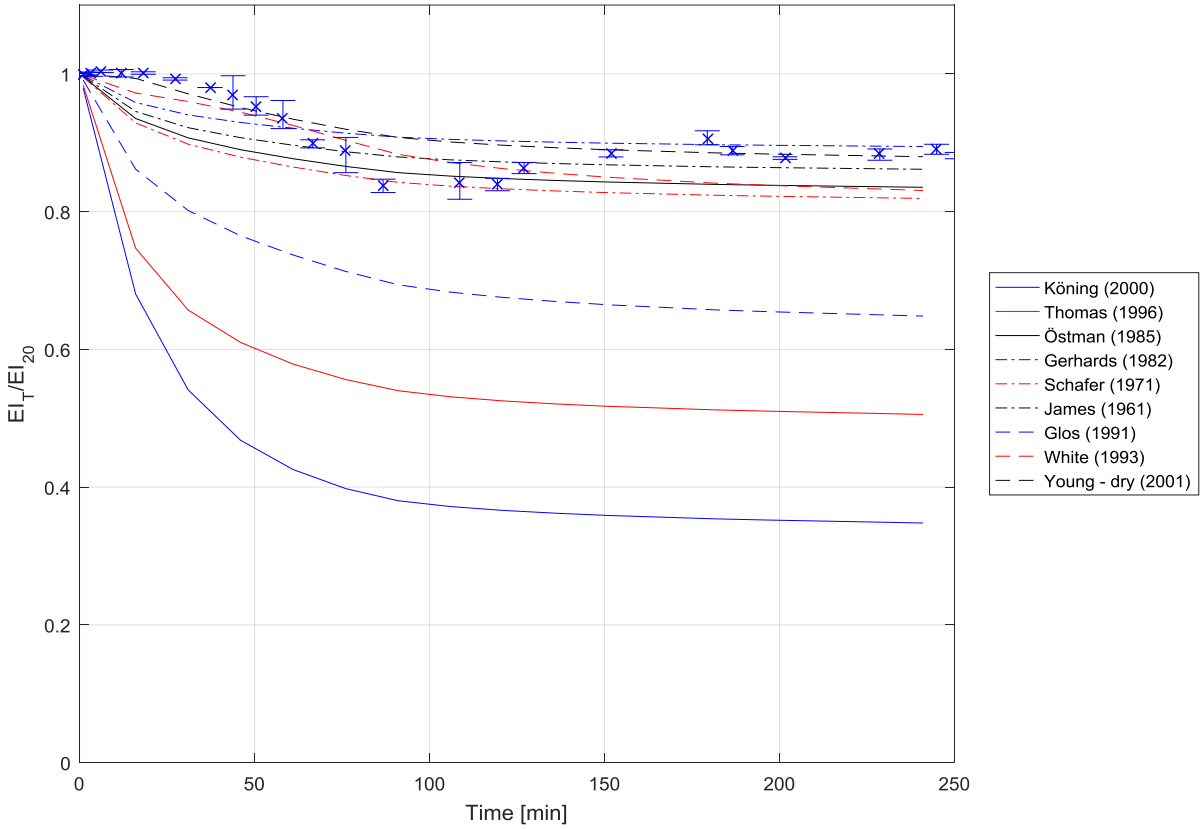

Figure. 39 Comparison of the stiffness reduction measured for Test 1 and values obtained using the model with different modulus of elasticity reduction functions

For Tests 1 and 4, a comparison has been made between the measured reduction of bending stiffness and results predicted by the thermal and stiffness models and they are presented on Figure. 39 and Figure 40. Even though none of the purposed modulus of elasticity reduction functions clearly represents the results obtained by the tests, it is evident that most of the function show a relatively good prediction. Biggest deviation are for functions purposed by Glos & Henrici (1991), Thomas (1996) and König (2000). It should be noted that function by König (2000), which was adopted in the EN 1995-1-2:2004 (E) (2004), shows the biggest overestimation of approximately 3 times bigger reduction of bending stiffness than the one measured here.

After the Test 1, when the heating system had been turned off and the beam had been left to cool down, unexpected behaviour has been observed. Namely, few minutes after the end of the test loud cracking noises were heard from the beam and upon later inspection of the beam delamination of layers has been observed (Figure 41). It happened on the bottom part of the beam on multiple places along the span and it was evident on both sides.

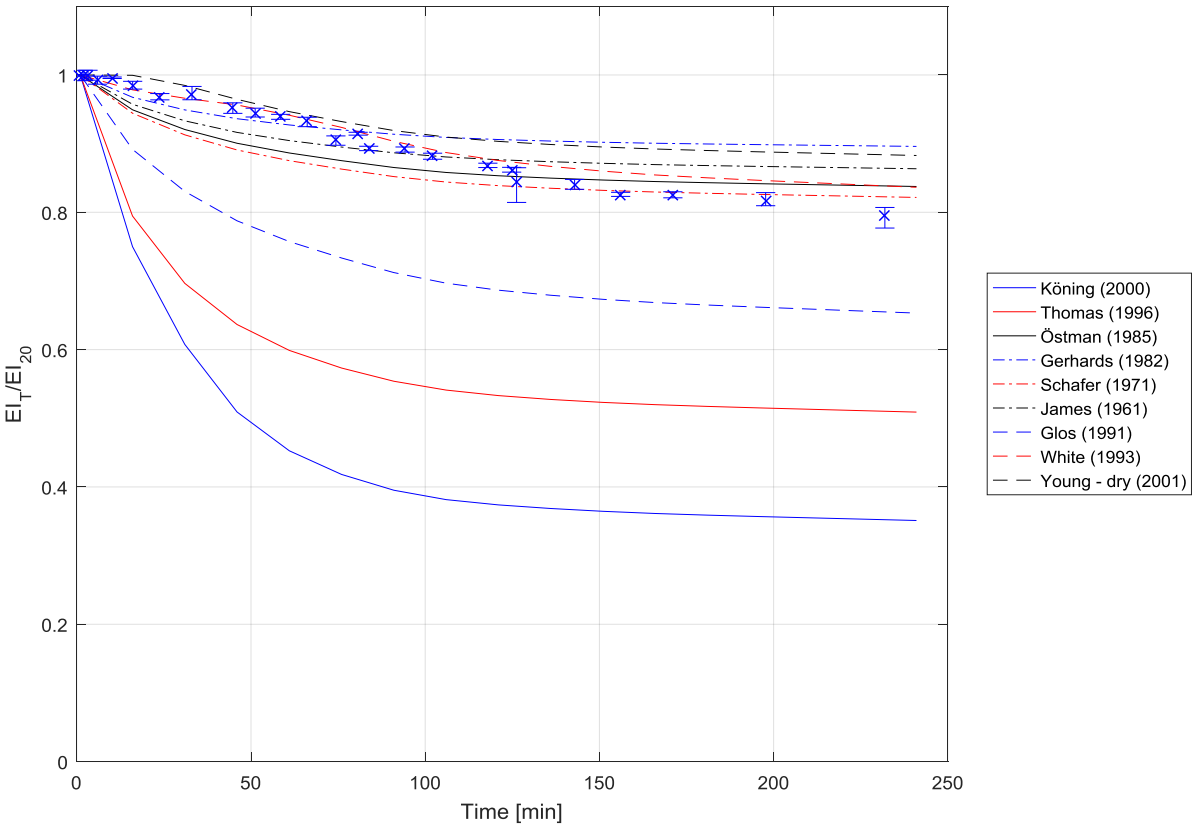

Figure 40 Comparison of the stiffness reduction measured for Test 1 and values obtained using the model with different modulus of elasticity reduction functions

This behaviour was not observed for other beam, except one short local delamination observed on the beam used in Test 2. This could possibly be the result of the fact that heating phase in the Test 1 lasted longer, approximately 6 hours, compared to other tests which lasted approximately 4 hours. The beams were not subjected to any mechanical load except for the self-weight and occasional impact excitation, but both loads were much lens intense than the capacity of the beam. This behaviour is alarming considering the fact that beams were not loaded and that the temperatures did not excide 140°C.

Figure 41 Delamination of layers observed on the bottom side of the beam used in Test 1 after cooling (both sides of the beam)

4. Conclusions

In this study, a thorough literature review was conducted in order to determine how the modulus of elasticity of timber changes with elevated temperature. The results in literature showed large variance, with the reported modulus of elasticity reduction varying form 4% to 80% at relatively low temperature of 100°C. This phenomenon is of great importance in predicting timber behaviour in fire conditions and needed further examination.

Almost all studies of this phenomenon were based on static measurements and obtained the modulus of elasticity from the recorded stress-strain diagram. This way of measuring does not isolate the effects of temperature as the creep and speed of applied load influence the measured deformation. In order to try excluding those influences from the evaluation of the behaviour of modulus of elasticity a novel way of testing using modal analysis was performed in this study.

Before conducting experiments, a numerical model was created in order to predict the results from experiments. The numerical model consisted of two parts, a thermal model and stiffness model. The thermal model was based on the finite difference method to evaluate temperature gradient inside the beam. Multiple sources for thermal properties were used and experimental validation showed that values provided in EN 1995-1-2:2004 (E) (2004) proved to be best for modelling thermal behaviour of timber beams used.

The stiffness model was based on modified “Sheer analogy” method and used multiple different function to describe the reduction of the modulus of elasticity with elevated temperature that were based on the findings from literature. The stiffness model showed possibility for relatively accurately determination of the reduction of modulus of elasticity based on the overall reduction of bending stiffness of the beam and so-called “effective” temperature of the cross section, which in the case of the samples used in this study was the temperature at 6 mm depth from the edge.

In order to validate the presented model, four experimental tests were conducted. Each consisted of heating the cross-laminated timber (CLT) beam with mounted thermocouples and high temperature accelerometer inside a specialised heating chamber. During the tests, while the beam was heating up, it would be excited by manually applying impulse force in order to cause oscillation. The acceleration was recorded using the accelerometer and based on that

data, using modal analysis, reduction of the stiffness during the tests was determined. This way dynamic modulus of elasticity behaviour with elevated temperature can be examined which should give more information into behaviour of the static modulus of elasticity isolated from added influences of creep.

Tests 1 and 4 showed relatively similar behaviour in the first 100 min of test, where in both tests the bending stiffness reduced by around 15%. After that, Test 1 showed unexpected behaviour, where the stiffness started to rise. For Test 4 stiffness continued to reduce similarly to the first part of the test.

Test 2 results were not deemed reliable as the obtained result varied too much. The source of this could potentially be found in the observed torsional deformation of the tested beam. This caused the beam not to rest ideally on the supports. During the oscillation, the beam also experienced torsional oscillation that could interfere with the measured acceleration and determination of stiffness.

In Test 3 unexpected behaviour was detected, where the measured beam stiffness increased upon heating the beam. The cause of this behaviour is not determined and it is not clear if it is the consequence of the actual material behaviour or an unexpected flaw of the testing procedure. Some possible resonance from the oscillation induced by the heating system were detected, but it is not clear if that could be the cause of the unforeseen results.

When results obtained from Test 1 and 4 were compared with the previously mentioned results from literature they showed relatively good correlation with sources that predicted smaller reduction, but on the other hand were greatly overpredicted by the widely used reduction which was adopted by EN 1995-1-2:2004 (E) (2004).

In order to properly validate this novel way of testing the reduction of stiffness at elevated temperature more tests should be conducted. In addition to use of full sized beams similar to the ones used in this study, smaller wood samples should be used. This way a uniform thermal gradient would be achieved and possibly a smaller influence of moisture transport. Furthermore, dynamic tests should be accompanied by static ones in order to more precisely determine the connection between the dynamic and static modulus of elasticity at elevated temperature. This way influence of creep could be studied more detailed.

References

Agilent Technologies. (2000). The Fundamentals of Signal Analysis. Application Note 243. *Agilent Technologies*. https://doi.org/AN-243

Benichou, N. (1999). *Fire Resistance of Lightweight Wood-Framed Assemblies : State-of-the-Art Report*. (January). https://doi.org/10.4224/20331309

BIS. (2010). *ESTIMATING THE AMOUNT OF CO2 EMISSIONS THAT THE CONSTRUCTION INDUSTRY CAN INFLUENCE Supporting material for the Low Carbon Construction IGT Report*. Retrieved from https://assets.publishing.service.gov.uk/government/uploads/system/uploads/attachment_data/file/31737/10-1316-estimating-co2-emissions-supporting-low-carbon-igt-report.pdf

Blass, H. J., & Fellmoser, P. (2004). Design of solid wood panels with cross layers. *8th World Conference on Timber Engineering*.

Drysdale, D. (2011). An Introduction to Fire Dynamics: Third Edition. In *An Introduction to Fire Dynamics: Third Edition*. https://doi.org/10.1002/9781119975465

EN 1991-1-2:2004 (E). (2004). *Eurocode 1 — Actions on structures Part 1-2: Actions on structures exposed to fire*.

EN 1995-1-1:2004 (E). (2004). *Eurocode 5 — Design of timber structures Part 1-1: General — Common rules and rules for buildings*. Eurocode 5 – Design of timber structures.

EN 1995-1-2:2004 (E). (2004). Eurocode 5 – Design of timber structures Part 1-2: General – Structural fire design. *Eurocode 5 – Design of Timber Structures*.

Fredlund, B. (1993). Modelling of heat and mass transfer in wood structures during fire. *Fire Safety Journal*. https://doi.org/10.1016/0379-7112(93)90011-E

Gagnon, S., & Pirvu, C. (2011). CLT Handbook: Cross-Laminated Timber. In *FPInnovations*. https://doi.org/10.1017/CBO9781107415324.004

Gerhards, C. C. (1982). Effect of moisture content and temperature on the mechanical properties of wood: an analysis of immediate effects. *October*. https://doi.org/10.1079/PHN2004659

Glos, P., & Henrici, D. (1991). Biegefestigkeit und Biege-E-Modul von Fichtenbauholz im Temperaturbereich bis 150°C. *Holz Als Roh- Und Werkstoff*. https://doi.org/10.1007/BF02619461

Green, M., & Karsh, E. (2012). The Case for Tall Wood Buildings. In *Tall Wood*.

H White, R., Cramer, S., & Shrestha, D. (2019). *Fire Endurance Model for a Metal-Plate-Connected Wood Truss*.

Hua, Y., & Sarkar, T. K. (1990). Matrix Pencil Method for Estimating Parameters of Exponentially Damped/Undamped Sinusoids in Noise. *IEEE Transactions on Acoustics, Speech, and Signal Processing*. https://doi.org/10.1109/29.56027

James, W. L. (1961). Effect of temperature and moisture content on internal friction and speed of sound in Douglas-fir. *Forest Products Journal*.

Janssens, M. L. (2004). Modeling of the thermal degradation of structural wood members exposed to fire. *Fire and Materials*. https://doi.org/10.1002/fam.848

Jong, F., & Clancy, P. (2004). Compression properties of wood as functions of moisture, stress and temperature. *Fire and Materials*, *28*(24), 209–225. https://doi.org/10.1002/fam.859

Knudson, M. (1975). *Performance of structural wood members exposed to fire /* (Vol. 25).

Kollmann, F. (1951). Technologie des Holzes und der Holzwerkstoffe. In *Zweite Auflage, erster Band*. https://doi.org/10.1007/978-3-642-52947-4

Kollmann, F., & Cote, W. A. (1968). Principles of wood science and technology I - Solid wood. In *Springer Verlag*. https://doi.org/10.1097/00010694-194311000-00010

König, J. (1991). Modelling the Effective Cross-Section of Timber Frame Members Exposed to Fire. *International Council for Building Research Studies and Documentation. Working Commission W18A - Timber Structures Meeting 24. Oxford, United Kingdom.*

König, J. (1994). Axially Loaded Timber Framed Walls Exposed to Fire on One Side. *Pacific Timber Engineering Conference. Gold Coast, Australia. Pp 263-272.*

König, J. (2000). *Timber frame assemblies exposed to standard and parametric fires. Part 2 A design model for standard fire exposure*.

LabVIEW. (2018). LabVIEW - National Instruments. *United States*.

MATLAB. (2016). MATLAB - Mathworks - MATLAB & Simulink. https://doi.org/2016-11-26

Östman, B. A. L. (1985). Wood tensile strength at temperatures and moisture contents simulating fire conditions. *Wood Science and Technology*. https://doi.org/10.1007/BF00353071

Ross, R. J., & USDA Forest Service., F. P. L. (2010). *Wood handbook : wood as an engineering material*. https://doi.org/10.2737/FPL-GTR-190

Schaffer, E. (1971). *ELEVATED TEMPERATURE EFFECT ON THE LONGITUDINAL MECHANICAL PROPERTIES OF WOOD*. Retrieved from http://search.proquest.com/docview/302554216/

Schaffer, E. L. (1986). *Strength validation and fire endurance of glued-laminated timber beams*. Retrieved from http://hdl.handle.net/2027/umn.31951d02988976z

SFPE. (2012). *Draft Guidelines for Designing Fire Safety in Very Tall Buildings* (p. 154). p. 154.

Public Rev. Society of Fire Protection Engineers.

Thomas, G. C. (1996). *Fire resistance of light timber framed walls and floors.* Retrieved from https://ir.canterbury.ac.nz/handle/10092/5877

WHO | Urban population growth. (2015). Retrieved April 7, 2019, from WHO website: https://www.who.int/gho/urban_health/situation_trends/urban_population_growth_text/en/

Young, S. A., & Clancy, P. (2001). Compression mechanical properties of wood at temperatures simulating fire conditions. *Fire and Materials*, *25*(3), 83–93. https://doi.org/10.1002/fam.759

Zieliński, T. P., & Duda, K. (2011). Frequency and damping estimation methods - An overview. *Metrology and Measurement Systems*. https://doi.org/10.2478/v10178-011-0051-y

Appendix

Comparison of the temperature modelled and recorded for Test 2

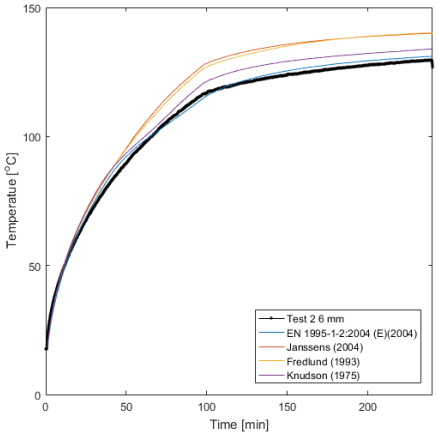

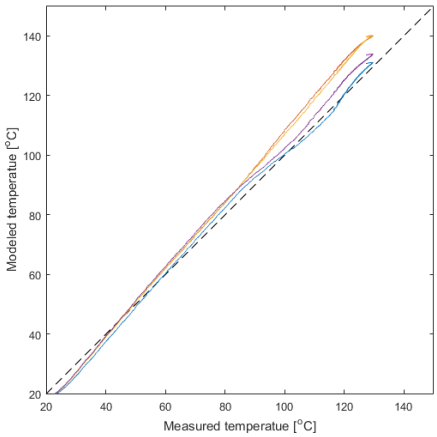

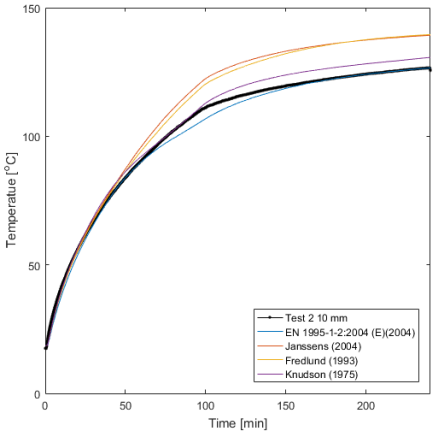

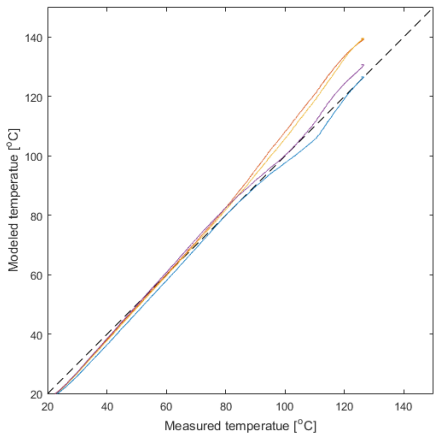

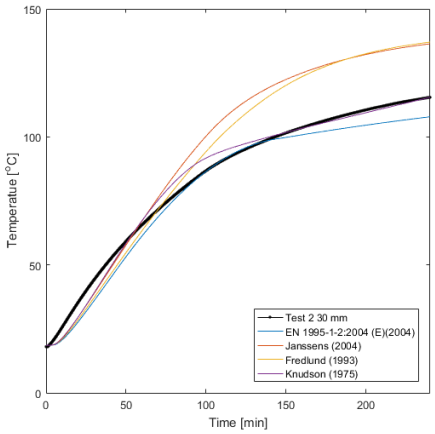

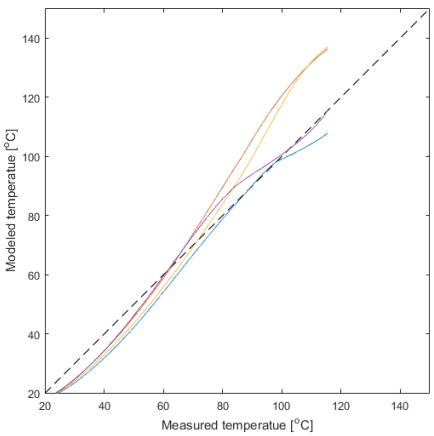

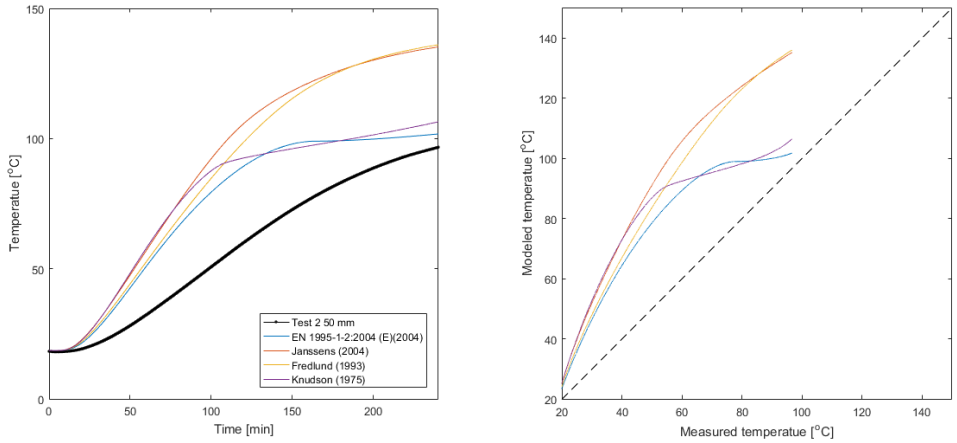

Comparison of the temperature modelled and recorded for Test 3

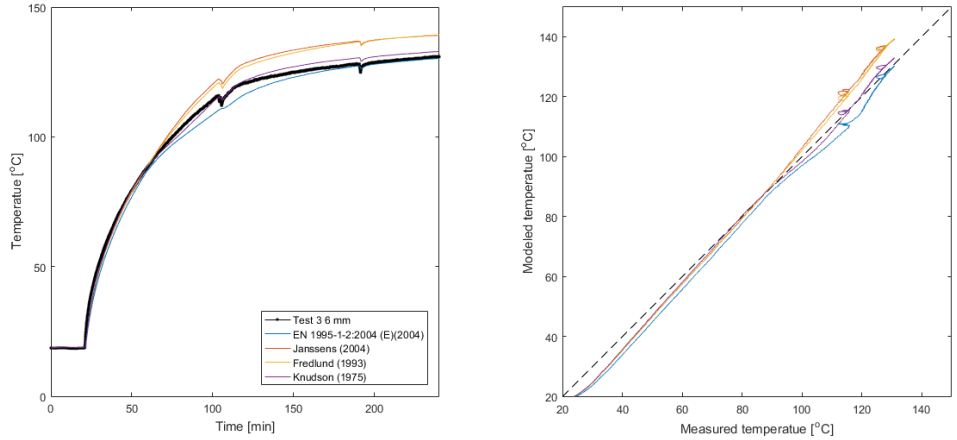

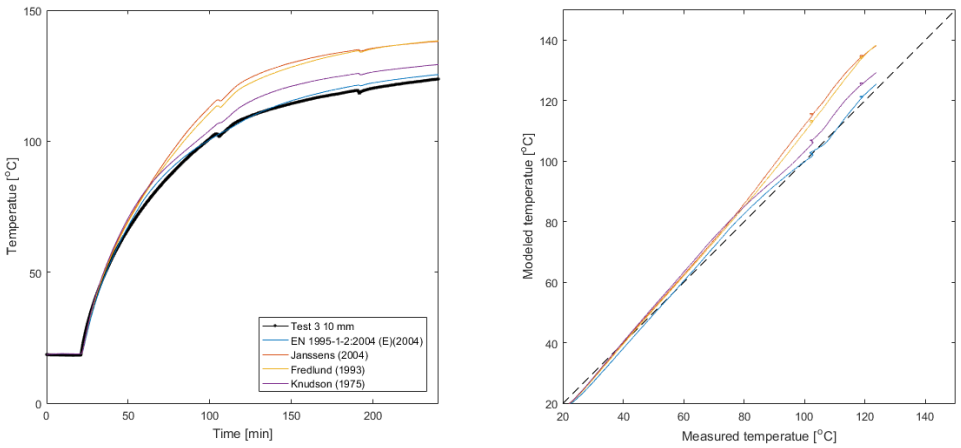

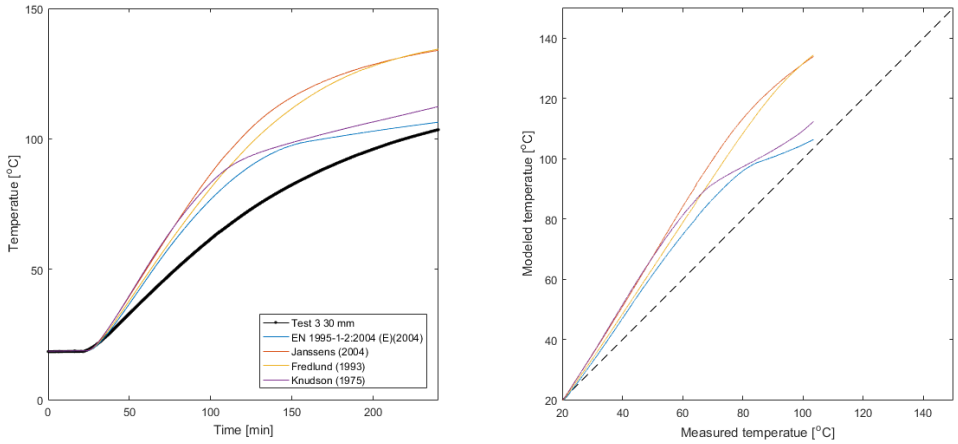

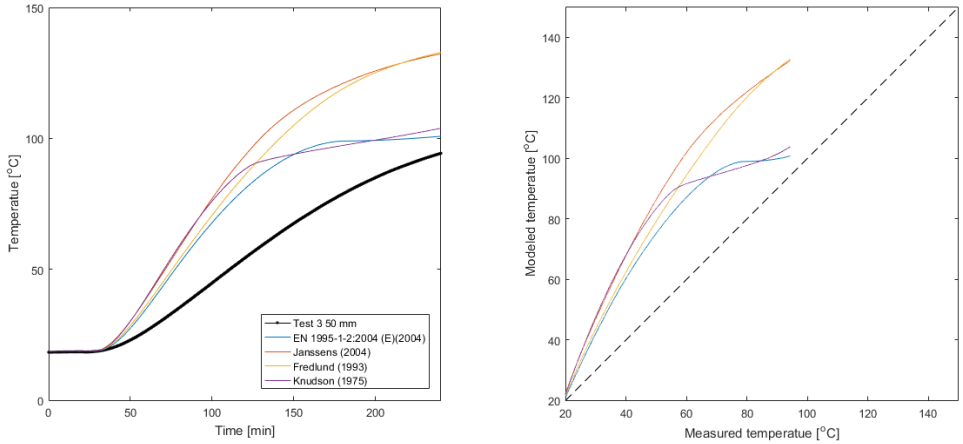

Comparison of the temperature modelled and recorded for Test 4

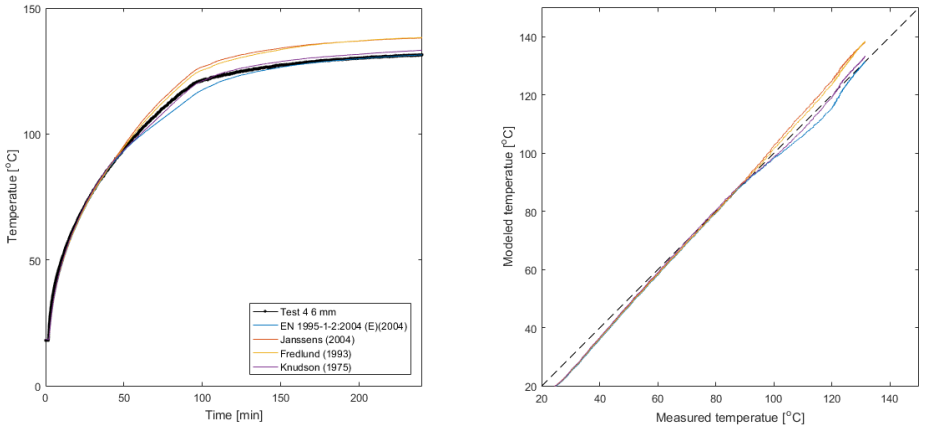

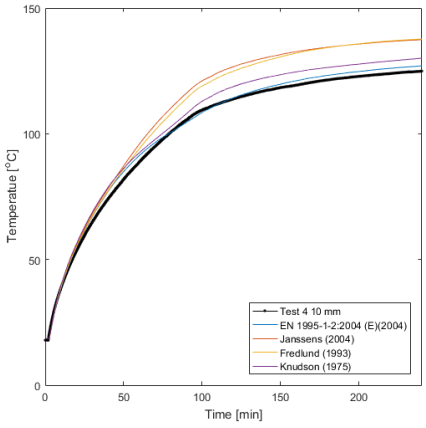
Temperatue [°C]
Time [min]
Test 4 10 mm
EN 1995-1-2:2004 (E)(2004)
Janssens (2004)
Fredlund (1993)
Knudson (1975)

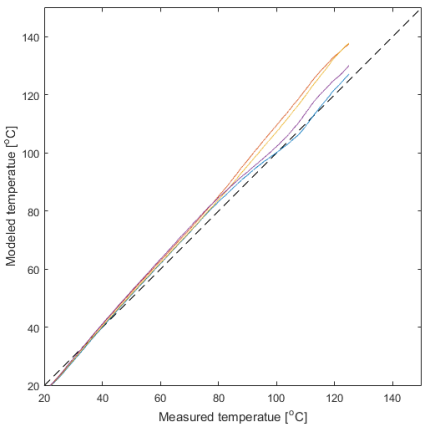
Modeled temperatue [°C]
Measured temperatue [°C]

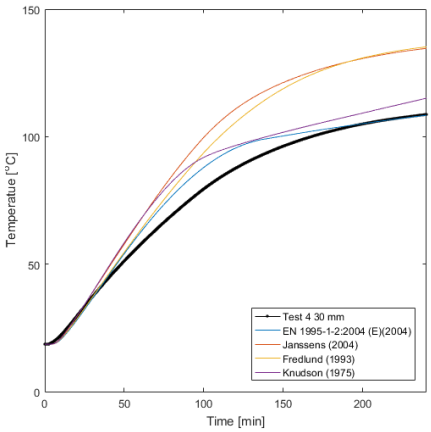
Temperatue [°C]
Time [min]
Test 4 30 mm
EN 1995-1-2:2004 (E)(2004)
Janssens (2004)
Fredlund (1993)
Knudson (1975)

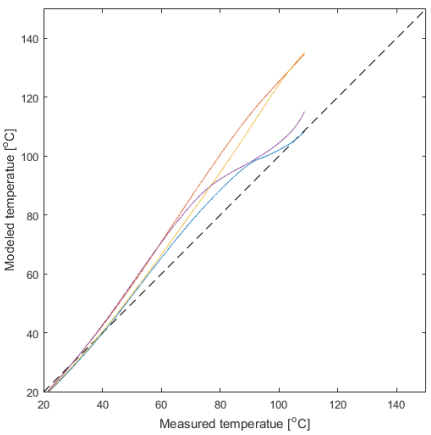
Modeled temperatue [°C]
Measured temperatue [°C]

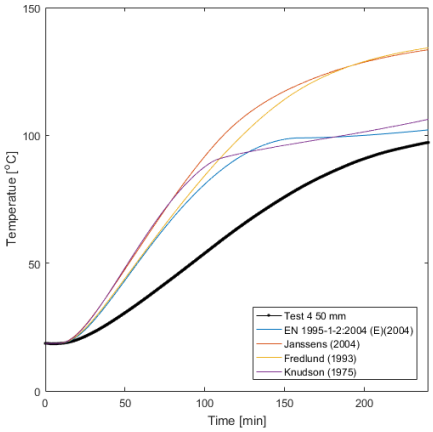
Temperatue [°C]
Time [min]
Test 4 50 mm
EN 1995-1-2:2004 (E)(2004)
Janssens (2004)
Fredlund (1993)
Knudson (1975)

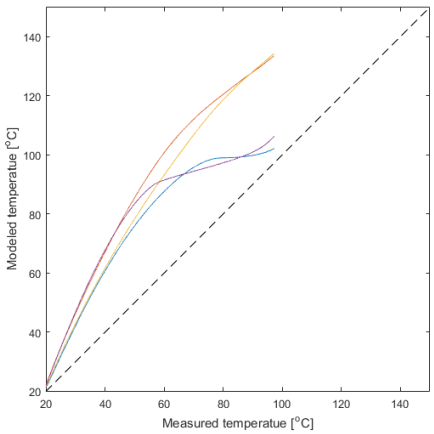
Modeled temperatue [°C]
Measured temperatue [°C]

Measured Temperature on the oustise of the longitudinal axes of the beam for Test 1

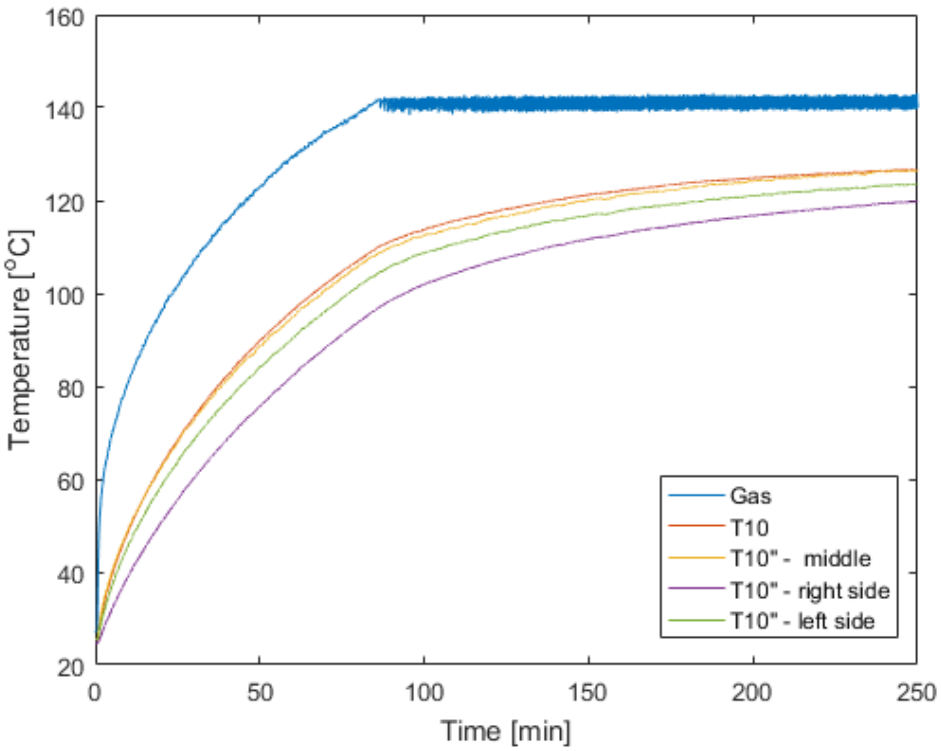

Measured Temperature on the oustise of the longitudinal axes of the beam for Test 2

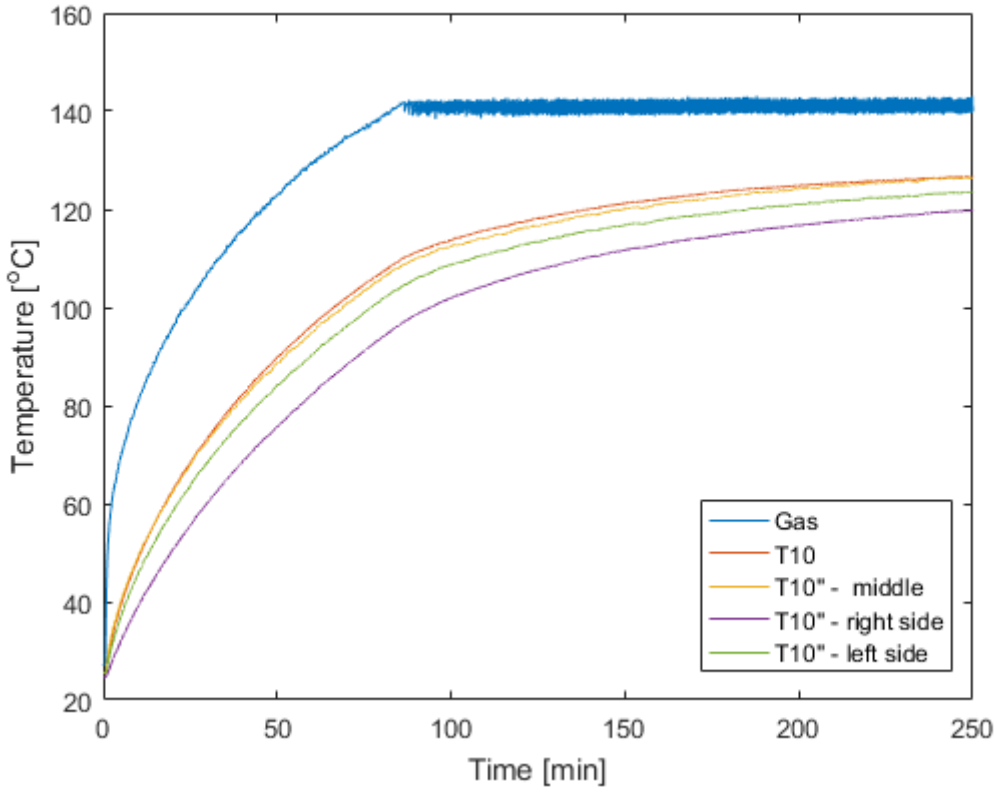

Measured Temperature on the oustise of the longitudinal axes of the beam for Test 3

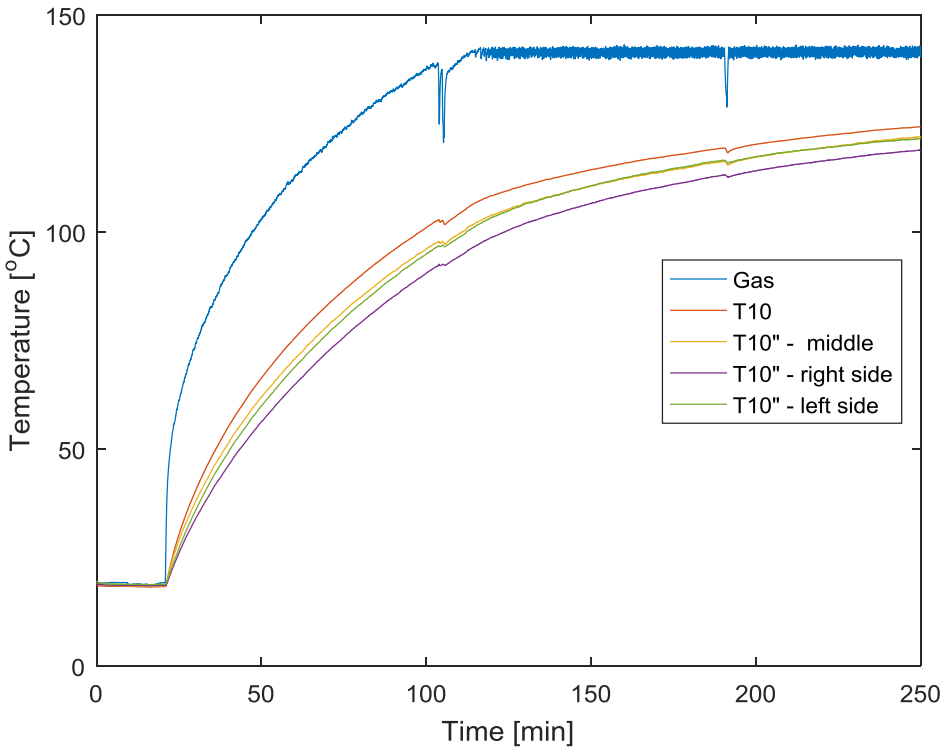

Measured Temperature on the oustise of the longitudinal axes of the beam for Test 1